PSelInv—A Distributed Memory Parallel Algorithm for Selected Inversion: The Symmetric Case

MATHIAS JACQUELIN, Lawrence Berkeley National Laboratory
LIN LIN, University of California, Berkeley and Lawrence Berkeley National Laboratory
CHAO YANG, Lawrence Berkeley National Laboratory

We describe an efficient parallel implementation of the selected inversion algorithm for distributed memory computer systems, which we call PSelInv. The PSelInv method computes selected elements of a general sparse matrix A that can be decomposed as $A = LU$, where L is lower triangular and U is upper triangular. The implementation described in this article focuses on the case of sparse symmetric matrices. It contains an interface that is compatible with the distributed memory parallel sparse direct factorization SuperLU_DIST. However, the underlying data structure and design of PSelInv allows it to be easily combined with other factorization routines, such as PARDISO. We discuss general parallelization strategies such as data and task distribution schemes. In particular, we describe how to exploit the concurrency exposed by the elimination tree associated with the LU factorization of A. We demonstrate the efficiency and accuracy of PSelInv by presenting several numerical experiments. In particular, we show that PSelInv can run efficiently on more than 4,000 cores for a modestly sized matrix. We also demonstrate how PSelInv can be used to accelerate large-scale electronic structure calculations.

Categories and Subject Descriptors: G.4 [**Mathematical Software**]: *Algorithm design and analysis*; G.4 [**Mathematical Software**]: *Parallel and vector implementations*; I.1.2 [**Symbolic and Algebraic Manipulation**]: Algorithms—*Algebraic algorithms*

General Terms: Design, Performance

Additional Key Words and Phrases: Selected inversion, sparse direct method, distributed memory parallel algorithm, high-performance computation, electronic structure theory

ACM Reference Format:
Mathias Jacquelin, Lin Lin, and Chao Yang. 2016. PSelInv—A distributed memory parallel algorithm for selected inversion: The symmetric case. ACM Trans. Math. Softw. 43, 3, Article 21 (November 2016), 28 pages.
DOI: http://dx.doi.org/10.1145/2786977

1. INTRODUCTION

Let $A \in \mathbb{C}^{N\times N}$ be a nonsingular sparse matrix. We are interested in computing *selected elements* of A^{-1}, defined as

$$\{(A^{-1})_{i,j}| \ \text{for} \ 1 \le i, j \le N \ \text{such that} \ A_{i,j} \neq 0\}. \tag{1}$$

This work was partially supported by the Laboratory Directed Research and Development Program of Lawrence Berkeley National Laboratory under U.S. Department of Energy contract DE-AC02-05CH11231 (L. L. and C. Y.), the Scientific Discovery through Advanced Computing (SciDAC) program funded by the U.S. Department of Energy, Office of Science, Advanced Scientific Computing Research and Basic Energy Sciences (M. J., L. L., and C. Y.), and the Center for Applied Mathematics for Energy Research Applications (CAMERA), which is a partnership between Basic Energy Sciences (BES) and Advanced Scientific Computing Research (ASRC) at the U.S Department of Energy.
Q1 Authors' addresses:
Permission to make digital or hard copies of part or all of this work for personal or classroom use is granted without fee provided that copies are not made or distributed for profit or commercial advantage and that copies show this notice on the first page or initial screen of a display along with the full citation. Copyrights for components of this work owned by others than ACM must be honored. Abstracting with credit is permitted. To copy otherwise, to republish, to post on servers, to redistribute to lists, or to use any component of this work in other works requires prior specific permission and/or a fee. Permissions may be requested from Publications Dept., ACM, Inc., 2 Penn Plaza, Suite 701, New York, NY 10121-0701 USA, fax +1 (212) 869-0481, or permissions@acm.org.
© 2016 ACM 0098-3500/2016/11-ART21 $15.00
DOI: http://dx.doi.org/10.1145/2786977

32 Sometimes we only need to compute a subset of these selected elements—for example,
33 the diagonal elements of A^{-1}. The most straightforward way to obtain these selected
34 elements of A^{-1} is to compute the full inverse of A and then extract the selected
35 elements. But this is often prohibitively expensive in practice. It turns out that to
36 compute these selected elements of A^{-1}, some additional elements of A^{-1} often need to
37 be computed. However, the overall set of nonzero elements that need to be computed
38 often remains a small percentage of all elements of A^{-1} due to the sparsity structure
39 of A.

40 The selected elements of A^{-1} defined by (1) can be used to obtain trace estimation of
41 the form

$$\mathrm{Tr}[A^{-1}] \quad \text{or} \quad \mathrm{Tr}[A^{-1}B^T], \tag{2}$$

42 if the sparsity pattern of $B \in \mathbb{C}^{N\times N}$ is contained in the sparsity pattern of A (i.e.,
43 $\{(i,j)|B_{i,j} \neq 0\} \subset \{(i,j)|A_{i,j} \neq 0\}$). The computation of selected elements of A^{-1} together
44 with the trace estimation of the form (2) arise in several scientific computing appli-
45 cations, including density functional theory (DFT) [Hohenberg and Kohn 1964; Kohn
46 and Sham 1965], dynamical mean-field theory (DMFT) [Kotliar et al. 2006], Poisson-
47 Boltzmann equations [Xu and Maggs 2013], and uncertainty quantification [Bekas
48 et al. 2009].

49 It is possible to compute selected elements of A^{-1} by iterative methods such as the
50 Lanczos algorithm [Lanczos 1950; Sidje and Saad 2011], combined with Monte Carlo
51 [Bekas et al. 2007] or deterministic probing techniques [Tang and Saad 2012]. These
52 types of methods work well if A^{-1} is a banded matrix or it becomes a banded matrix
53 after elements with absolute value less than ε have been truncated, and a sparse
54 factorization of A is prohibitively expensive to perform.

55 In this article, we focus on using a sparse direct method to compute selected elements
56 **Q2** of A^{-1}. We assume that a sparse LU factorization (or LDL^T factorization if A is sym-
57 metric) of A is computationally feasible. The main advantage of a direct method is that
58 we do not need to make assumptions on the decay property of A^{-1}. The disadvantage
59 of this direct method is that it actually computes a superset of the selected elements of
60 A^{-1} as defined in Equation (1). In particular, all elements of A^{-1} indexed by the union
61 of the nonzero index sets of the L and U factors need to be computed. It should be noted
62 that as long as L and U remain sparse, computing elements of A^{-1} restricted to this
63 superset can still be much faster than computing the full inverse.

64 Sparse direct methods for computing selected elements of A^{-1} were first proposed
65 in Takahashi et al. [1973] and Erisman and Tinney [1975]. The use of an elimination
66 tree for computing selected elements of inverse was presented in Campbell and Davis
67 [1995] for a sequential algorithm. Motivated by quantum transport simulations, Li
68 et al. [2008], Li and Darve [2012], and Li et al. [2013] developed the fast inverse
69 using nested dissection (FIND) algorithm for computing the diagonal of A^{-1}. Some
70 related work has been described in Cauley et al. [2012] and Eastwood and Wan [2013].
71 The FIND algorithm is in principle applicable to matrices with a general sparsity
72 pattern, but so far its implementation focuses on structured matrices obtained from
73 second-order partial differential operators discretized by a finite difference scheme.
74 The implementation of FIND is not yet publicly available. Nor is it scalable to a large
75 number of processors. Lin et al. [2009b] developed the hierarchically Schur complement
76 (HSC) method for a similar type of matrix arising from DFT-based electronic structure
77 calculations. The method has also been generalized and applied to quantum transport
78 calculations [Hetmaniuk et al. 2013].

79 An efficient implementation of the selected inversion algorithm for a general sym-
80 metric matrix, called `SelInv`, was presented in Lin et al. [2011b] and is publicly avail-
81 able. Amestoy et al. [2012a] considered a more general parallel matrix inversion method

for computing any subset of entries of A^{-1}. They implemented their algorithm in the MUMPS package [Amestoy et al. 2001], which is based on the multifrontal method. In this algorithm, the actual set of computed entries of A^{-1} contains entries on the critical path of the requested entries to the root of the elimination tree, and therefore this is also a superset of the requested entries of A^{-1}. This method is more efficient than our algorithm when a small number of entries of A^{-1} are requested. However, when a relatively large number of entries are to be computed, such as in the computation of the selected elements defined by (1), our algorithm can more efficiently reuse the information shared among different entries of A^{-1}, and our numerical results indicate that our algorithm is more efficient than the parallel matrix inversion method implemented in MUMPS. In addition to the work presented in Amestoy et al. [2012a, 2012b], parallel implementation of algorithms for computing selected elements of inverse tailored to matrices obtained from a finite difference discretization of a second-order partial differential operator have appeared in several publications [Petersen et al. 2009; Lin et al. 2011a]. The method developed by Petersen et al. [2009], which was designed for a quasi-1D quantum transport problem, is scalable to a relatively small ($32 \sim 64$) number of processors. In Lin et al. [2011a], we described an efficient parallel implementation for discretized 2D Laplacian-type operators and demonstrated the efficiency of the implementation when it was used to solve a problem with billions of degrees of freedom on 4,096 processors. However, this implementation cannot be used to perform a selected inversion of a general symmetric sparse matrix with an arbitrary sparsity pattern.

The purpose of this article is to extend the selected inversion algorithm presented in Lin et al. [2011b] and describe an implementation of a parallel selected inversion algorithm designed for distributed memory parallel computers. Such an implementation allows us to solve much larger problems by utilizing more computational resources available on high-performance computers. The present work is more general than the previous work in Lin et al. [2011a], which assumes a balanced binary elimination tree and is only applicable to structured sparse matrices obtained from finite difference discretization of differential operators. It can utilize far greater numbers of processors than the sequential algorithm described in Lin et al. [2011b] for general sparse matrices.

The parallel implementation of the selected inversion algorithm that we present in this article uses a more general data distribution and communication strategy to divide the work among a large number of processors to achieve multiple levels of concurrency. We name our implementation PSelInv, and the software is publicly available.[1] Our first implementation focuses on the case of sparse symmetric matrices. In principle, the PSelInv package can be interfaced with any sparse LU and LDL^T factorization routines. Our current implementation provides an interface to the SuperLU_DIST [Li and Demmel 2003] package. The user has the option of using either the ParMETIS [Karypis and Kumar 1998] software or the PT-Scotch [Chevalier and Pellegrini 2008] package to reorder the matrix in parallel to minimize the nonzero fill in the sparse matrix factors.

The rest of the article is organized as follows. We review the basic idea of the selected inversion method in Section 2 and discuss various implementation issues for the distributed memory parallel selected inversion algorithm in Section 3. The numerical results with applications to various matrices from the Harwell-Boeing Test Collection [Duff et al. 1992] and the University of Florida Matrix Collection [Davis and Hu 2011],

[1]http://www.pexsi.org/, distributed under the BSD license.

Q3

130 and also applications from DFT, are given in Section 4, followed by our conclusions and
131 the discussion of future work in Section 5.
132 Standard linear algebra notation is used for vectors and matrices throughout the
133 article. We use $A_{i,j}$ to denote the (i, j)-th entry of the matrix A and f_i to denote the i-th
134 entry of the vector f. With slight abuse of notation, both a supernode index and the set
135 of column indices associated with a supernode are denoted by uppercase script letters,
136 such as $\mathcal{I}, \mathcal{J}, \mathcal{K}$. Furthermore, we use $A_{i,*}$ and $A_{*,j}$ to denote the i-th row and the j-th
137 column of A, respectively. Similarly, $A_{\mathcal{I},*}$ and $A_{*,\mathcal{J}}$ are used to denote the $\mathcal{I}$-th block row
138 and the $\mathcal{J}$-th block column of A, respectively. $A^{-1}_{\mathcal{I},\mathcal{J}}$ denotes the $(\mathcal{I}, \mathcal{J})$-th block of the
139 matrix A^{-1} (i.e., $A^{-1}_{\mathcal{I},\mathcal{J}} \equiv (A^{-1})_{\mathcal{I},\mathcal{J}}$). When the block $A_{\mathcal{I},\mathcal{J}}$ itself is invertible, its inverse is
140 denoted by $(A_{\mathcal{I},\mathcal{J}})^{-1}$ to distinguish it from $A^{-1}_{\mathcal{I},\mathcal{J}}$.

141 ## 2. SELECTED INVERSION ALGORITHM

142 ### 2.1. Basic Formulation

143 Although this article focuses on the computation of selected elements of A^{-1} when A is a
144 sparse symmetric matrix, the idea of the selected inversion algorithm can be given for a
145 general square matrix A and will be used in our ongoing work for computing the selected
146 elements of A^{-1} for asymmetric matrices. The standard approach for computing A^{-1} is
147 to first decompose the general matrix A using the LU factorization

$$A = LU, \tag{3}$$

148 where L is a unit lower triangular matrix and U is an upper triangular matrix. To
149 stabilize the computation, matrix reordering and partial pivoting [Golub and Van Loan
150 1996] are usually applied to the matrix of A, and the general form of the LU factorization
151 can be given as

$$PAQ = LU, \tag{4}$$

152 where P and Q are two permutation matrices. To simplify the discussion, we will use
153 Equation (3) and assume that A has already been permuted.
154 Given the LU factorization, the most straightforward way to compute selected
155 elements of A^{-1} is to obtain $A^{-1} \equiv (x_1, x_2, \ldots, x_n)$ by solving several triangular
156 systems

$$Ly_j = e_j, \quad Ux_j = y_j, \tag{5}$$

157 where $j = 1, 2, \ldots, n$, and e_j is the j-th column of the $n \times n$ identity matrix. Such
158 a procedure, which will be referred to as the direct inversion algorithm, is generally
159 very costly even when A is sparse. The direct inversion algorithm performs too much
160 computation when only a small number of selected elements of the inverse matrix are
161 needed.
162 An alternative algorithm is the selected inversion algorithm, which accurately com-
163 putes all selected elements of A^{-1}. The idea of the selected inversion method originates
164 from Takahashi et al. [1973] and Erisman and Tinney [1975], and the algorithm and
165 its variants have been discussed in several works [Lin et al. 2009b; Lin et al. 2011b;
166 Amestoy et al. 2012b; Li et al. 2008; Li and Darve 2012; Kuzmin et al. 2013]. The se-
167 lected inversion algorithm can be understood as follows. We first partition the matrix
168 A into 2×2 blocks of the form

$$A = \begin{pmatrix} A_{1,1} & A_{1,2} \\ A_{2,1} & A_{2,2} \end{pmatrix}, \tag{6}$$

where $A_{1,1}$ is a scalar of size 1×1. We can write $A_{1,1}$ as a product of two scalars $L_{1,1}$ and $U_{1,1}$. In particular, we can pick $L_{1,1} = 1$ and $U_{1,1} = A_{1,1}$. Then

$$A = \begin{pmatrix} L_{1,1} & 0 \\ L_{2,1} & I \end{pmatrix} \begin{pmatrix} U_{1,1} & U_{1,2} \\ 0 & S_{2,2} \end{pmatrix}, \tag{7}$$

where

$$L_{2,1} = A_{2,1}(U_{1,1})^{-1}, \quad U_{1,2} = (L_{1,1})^{-1} A_{1,2}. \tag{8}$$

The L and U factors are usually directly accessible in a standard LU factorization, and

$$S_{2,2} = A_{2,2} - L_{2,1} U_{1,2} \tag{9}$$

is the Schur complement. Using the decomposition given by Equation (7), we can express A^{-1} as

$$A^{-1} = \begin{pmatrix} (U_{1,1})^{-1}(L_{1,1})^{-1} + (U_{1,1})^{-1} U_{1,2} S_{2,2}^{-1} L_{2,1} (L_{1,1})^{-1} & -(U_{1,1})^{-1} U_{1,2} S_{2,2}^{-1} \\ -S_{2,2}^{-1} L_{2,1} (L_{1,1})^{-1} & S_{2,2}^{-1} \end{pmatrix}. \tag{10}$$

Since $S_{2,2}$ is the same as S here, without ambiguity, $S_{2,2}^{-1} \equiv (S^{-1})_{2,2}$ can be used. To simplify the notation, we define the normalized LU factors as

$$\hat{L}_{1,1} = L_{1,1}, \quad \hat{U}_{1,1} = U_{1,1}, \quad \hat{L}_{2,1} = L_{2,1}(L_{1,1})^{-1}, \quad \hat{U}_{1,2} = (U_{1,1})^{-1} U_{1,2}, \tag{11}$$

and Equation (10) can be equivalently given by

$$A^{-1} = \begin{pmatrix} (\hat{U}_{1,1})^{-1}(\hat{L}_{1,1})^{-1} + \hat{U}_{1,2} S_{2,2}^{-1} \hat{L}_{2,1} & -\hat{U}_{1,2} S_{2,2}^{-1} \\ -S_{2,2}^{-1} \hat{L}_{2,1} & S_{2,2}^{-1} \end{pmatrix}. \tag{12}$$

Let us denote by $\mathcal{C}$ the set of indices

$$\{i | \left(L_{2,1}\right)_i \neq 0\} \cup \{j | \left(U_{1,2}\right)_j \neq 0\}, \tag{13}$$

and assume that $S_{2,2}^{-1}$ has already been computed. From Equation (12), it can be readily observed that to compute the i-th element of $A_{2,1}^{-1} \equiv -S_{2,2}^{-1} \hat{L}_{2,1}$ for $i \in \mathcal{C}$, we only need the entries

$$\left\{ \left(S_{2,2}^{-1}\right)_{i,j} | i \in \mathcal{C}, j \in \mathcal{C} \right\}. \tag{14}$$

The same set of entries of $S_{2,2}^{-1}$ are required to compute selected entries of $A_{1,2}^{-1} \equiv -\hat{U}_{1,2} S_{2,2}^{-1}$. No additional entries of $S_{2,2}^{-1}$ are needed to complete the computation of $A_{1,1}^{-1}$, which involves the matrix product of selected entries of $\hat{U}_{1,2}$ and $A_{2,1}^{-1}$. This procedure can be repeated recursively to compute selected elements of $S_{2,2}^{-1}$ until $S_{2,2}$ is a scalar of size 1. A pseudocode for demonstrating this column-based selected inversion algorithm for symmetric matrix is given in Lin et al. [2011b].

In practice, a column-based sparse factorization and selected inversion algorithm may not be efficient due to the lack of level 3 BLAS operations. For a sparse matrix A, the columns of A and the L factor can be partitioned into supernodes. A supernode is a maximal set of contiguous columns $\mathcal{J} = \{j, j+1, \ldots, j+s\}$ of the L factor that have the same nonzero structure below the $(j+s)$-th row, and the lower triangular part of $L_{\mathcal{J},\mathcal{J}}$ is dense. However, this strict definition can produce supernodes that are either too large or too small, leading to memory usage, load balancing, and efficiency issues. Therefore, in our work, we relax this definition to limit the maximal number

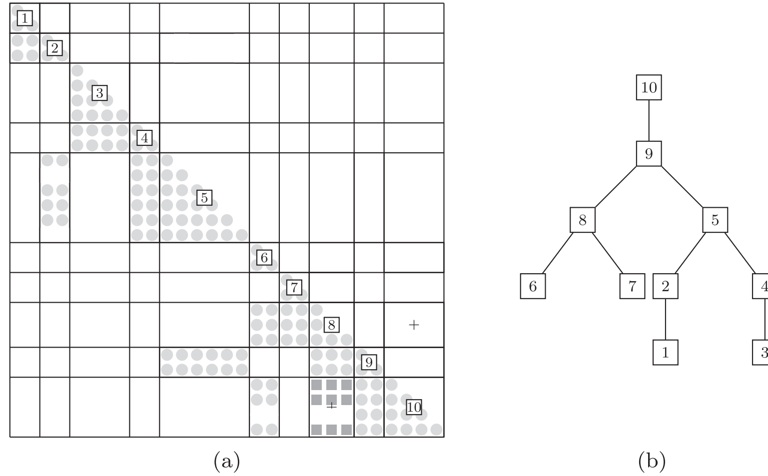

Fig. 1. (a) A structurally symmetric matrix A of size 29×29 divided into 10 supernodes. The nonzero matrix elements in A are labeled as round dots, and the extra fill-in elements in L are labeled as squares. (b) The elimination tree corresponding to the matrix A and its supernode partitioning.

of columns in a supernode (i.e., sets are not necessarily maximal). The relaxation also allows a supernode to include columns for which nonzero patterns are nearly identical to enhance the efficiency [Ashcraft and Grimes 1989]. This approach is also used in SuperLU_DIST [Li and Demmel 2003]. Even though the nonzero pattern of the matrix can be nonsymmetric, the same supernode partitioning is usually applied to the row partition as well, and we assume that the factorization has been computed using the structure of $A + A^T$. Then the nonzero structures of L and U are the transpose of each other. The total number of supernodes is denoted by $\mathcal{N}$. An example of the supernode partitioning of a structurally symmetric matrix A together with the extra fill-in in its L factor (U factor omitted due to structural symmetry) are given in Figure 1(a).

Using the notation of supernodes, a pseudocode for the selected inversion algorithm is given in Algorithm 1. The key step to gain computational efficiency in the selected inversion algorithm is step 2, which identifies the collection of all nonzero row and column indices corresponding to the supernode $\mathcal{K}$, denoted by $\mathcal{C}$. All subsequent steps operate only on these nonzero rows and columns within the sparsity pattern of the selected elements, thereby significantly reducing the computational cost.

It should be noted that if A is a sparse symmetric matrix, the normalized LU factors satisfy the relation

$$\hat{U}_{\mathcal{C},\mathcal{K}} = \hat{L}^T_{\mathcal{K},\mathcal{C}}. \tag{15}$$

To simplify the implementation, the entire diagonal block $A^{-1}_{\mathcal{K},\mathcal{K}}$ is computed even though it is symmetric. Due to round-off error, the numerical update in step 4 may not preserve this symmetry in finite precision. Our numerical results indicate that the loss of symmetry may accumulate, especially for ill-conditioned matrices. To reduce such error for symmetric matrices, we can simply symmetrize the diagonal block of A^{-1} by performing $A^{-1}_{\mathcal{K},\mathcal{K}} \leftarrow \frac{1}{2}(A^{-1}_{\mathcal{K},\mathcal{K}} + A^{-T}_{\mathcal{K},\mathcal{K}})$ after step 4 for each $\mathcal{K}$.

Furthermore, it should be noted that in the symmetric case, Equation (12) can be simplified using an LDL^T factorization, which is more efficient than an LU factorization, where L is a unit lower triangular matrix and D is a block diagonal matrix consisting of 1×1 or 2×2 blocks. The simplification of the selected inversion algorithm

ALGORITHM 1: Selected Inversion Algorithm Based on LU Factorization. Q4

Input: (1) The supernode partition of columns of A: $\{1, 2, \ldots, \mathcal{N}\}$
(2) A supernodal LU factorization of A with (unnormalized) LU factors L and U.
Output: Selected elements of A^{-1}(i.e., $A^{-1}_{\mathcal{I},\mathcal{J}}$ such that $L_{\mathcal{I},\mathcal{J}}$ is not an empty block).
for $\mathcal{K} = \mathcal{N}, \mathcal{N}-1, \ldots, 1$ **do**
1 Find the collection of indices
$\mathcal{C} = \{\mathcal{I} \mid \mathcal{I} > \mathcal{K}, L_{\mathcal{I},\mathcal{K}}$ is a nonzero block$\} \cup \{\mathcal{J} \mid \mathcal{J} > \mathcal{K}, U_{\mathcal{K},\mathcal{J}}$ is a nonzero block$\}$
2 $\hat{L}_{\mathcal{C},\mathcal{K}} \leftarrow L_{\mathcal{C},\mathcal{K}}(L_{\mathcal{K},\mathcal{K}})^{-1}, \; \hat{U}_{\mathcal{K},\mathcal{C}} \leftarrow (U_{\mathcal{K},\mathcal{K}})^{-1}U_{\mathcal{K},\mathcal{C}}$
end
for $\mathcal{K} = \mathcal{N}, \mathcal{N}-1, \ldots, 1$ **do**
Find the collection of indices
$\mathcal{C} = \{\mathcal{I} \mid \mathcal{I} > \mathcal{K}, L_{\mathcal{I},\mathcal{K}}$ is a nonzero block$\} \cup \{\mathcal{J} \mid \mathcal{J} > \mathcal{K}, U_{\mathcal{K},\mathcal{J}}$ is a nonzero block$\}$
3 Calculate $A^{-1}_{\mathcal{C},\mathcal{K}} \leftarrow -A^{-1}_{\mathcal{C},\mathcal{C}}\hat{L}_{\mathcal{C},\mathcal{K}}$
4 Calculate $A^{-1}_{\mathcal{K},\mathcal{K}} \leftarrow U^{-1}_{\mathcal{K},\mathcal{K}}L^{-1}_{\mathcal{K},\mathcal{K}} - \hat{U}_{\mathcal{K},\mathcal{C}}A^{-1}_{\mathcal{C},\mathcal{K}}$
5 Calculate $A^{-1}_{\mathcal{K},\mathcal{C}} \leftarrow -\hat{U}_{\mathcal{K},\mathcal{C}}A^{-1}_{\mathcal{C},\mathcal{C}}$
end

with an LDL^T factorization can be found in Lin et al. [2011b]. For symmetric matrices, $A^{-1}_{\mathcal{K},\mathcal{C}}$ (step 5) is readily obtained as the transpose of $A^{-1}_{\mathcal{C},\mathcal{K}}$ without extra computation. 225 226

2.2. Elimination Tree 227

Both the factorization and the selected inversion can be conveniently described in terms of traversals of an elimination tree [Liu 1990]. Each node of the tree corresponds to a supernode of A. A node $\mathcal{R}$ is the parent of a node $\mathcal{K}$ if and only if 228 229 230

$$\mathcal{R} = \min\{\mathcal{I} > \mathcal{J} \mid L_{\mathcal{I},\mathcal{J}} \text{ is a nonzero block}\}. \tag{16}$$

An example of the elimination tree corresponding to the matrix in Figure 1(a) is given in Figure 1(b). 231 232

In the factorization procedure, the traversal of the elimination tree is a bottom-up process that starts from the leaves of the tree. A parent supernode cannot be factored until the supernodes associated with all of its children in the tree have been factored. This type of task dependency also determines the amount of concurrency that can be exploited to speed up the factorization on a parallel computer. 233 234 235 236 237

In the selected inversion procedure, the traversal of the elimination tree is a top-down process that starts from the root of the tree. Computing the selected elements in the $\mathcal{K}$-th supernode of A^{-1} requires the selected elements of A^{-1} already computed at ancestor nodes of $\mathcal{K}$, but not those computed at its sibling nodes and their descendants. Consequently, the selected inversion of supernodes that belong to two different branches of the elimination tree can in principle be carried out independently as long as the selected elements computed at supernodes above these branches have been passed to processors that are assigned to work on these branches. 238 239 240 241 242 243 244 245

3. DISTRIBUTED MEMORY PARALLEL SELECTED INVERSION ALGORITHM 246

In this article, we present the distributed memory PSelInv method. Our first implementation focuses on the case of symmetric matrices. For such matrices, the selected inversion algorithms described in Algorithm 1 require a sparse LU or LDL^T factorization of A to be available first. Here we use the SuperLU_DIST software package [Li and Demmel 2003] to obtain the LU factorization, which has been shown to be scalable to a large number of processors on distributed memory parallel machines. 247 248 249 250 251 252

The relatively simple data structure of SuperLU_DIST allows easy access to sparse L and U factors. However, the main ideas that we develop here can be combined with other sparse matrix solvers, such as MUMPS [Amestoy et al. 2001], and PARDISO [Schenk and Gartner 2006] as well, which provides the LDL^T functionality and can potentially be two times faster in the factorization phase. We also note that only symmetric permutation of the matrix A is allowed, even though SuperLU_DIST allows the column permutation to be different from the row permutation. In this work, to preserve the symmetry of the matrix, we do not perform the equilibration procedure often used in the LU factorization to modify poorly scaled matrix elements. In the current implementation of the PSelInv method, we explicitly take advantage of the symmetry of the matrix and only compute the lower triangular part of the selected elements of A^{-1}. However, our implementation is not optimal in terms of memory allocation in the sense that both the upper and lower triangular part of A^{-1} are stored. As will be seen in the following, such a strategy simplifies the communication pattern and efforts for bookkeeping in the case of 2D block cyclic data distribution and facilitates generalizing PSelInv to asymmetric matrices. We also note that the suboptimal memory allocation is not a severe limitation of the PSelInv method. The memory footprint of PSelInv can be further optimized for applications that are constrained by the memory usage. Our numerical results also indicate that the additional memory usage by PSelInv is relatively small compared to that used in other procedures, such as the parallel numerical factorization.

We use the same 2D block cyclic distribution scheme employed in SuperLU_DIST to partition and distribute both the L factor and the selected elements of A^{-1} to be computed. We will review the main features of this type of distribution in Section 3.1. In the 2D block cyclic distribution scheme, each supernode $\mathcal{K}$ is assigned to and partitioned among a subset of processors. However, computing the selected elements of A^{-1} contained in the supernode $\mathcal{K}$ requires retrieving previously computed selected elements of A^{-1} that belong to ancestors of $\mathcal{K}$ in the elimination tree. These selected elements may reside on other processors. As a result, communication is required to transfer data among different processors to complete steps 3, 4, and 5 of Algorithm 1 in each iteration. We will discuss how this is done in Section 3.2. The key to reducing communication cost and achieving scalable performance is to overlap communication with computation by using asynchronous point-to-point MPI functions, even though some of these communication events are collective in nature (e.g., broadcast and reduce) within a communication subgroup.

In addition to utilizing a fine-grain level of parallelism in computing A^{-1} for each supernode, we introduce a coarse-grain level of parallelism by exploiting the concurrency available in the elimination tree. This amounts to executing different iterates of the for loop in Algorithm 1 in parallel. Although the elimination tree may exhibit many independent tasks associated with supernodes that belong to different branches of the elimination tree, the 2D block cyclic distribution of L and A^{-1} may prevent these tasks from being performed completely simultaneously on different processors. The key to minimizing the dependency issue is to properly assign the order of computational tasks and to overlap computation and communication as much as possible. We will discuss our preliminary strategy for improving the parallel efficiency using the elimination tree in Section 3.3.

3.1. Distributed Data Layout and Structure

As discussed in Section 2, the columns of A, L, and U are partitioned into supernodes. Different supernodes may have different sizes. The same partition is applied to the rows of these matrices to create a 2D block partition of these matrices. The submatrix blocks are mapped to processors that are arranged in a virtual 2D grid of dimension

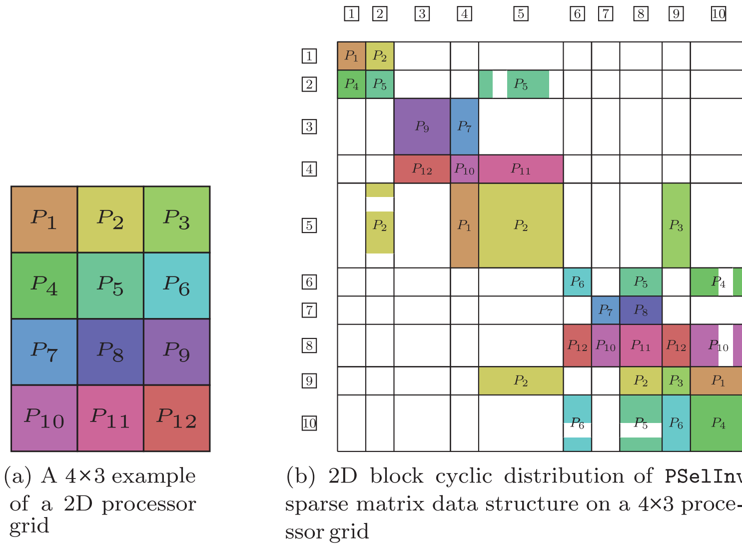

(a) A 4×3 example of a 2D processor grid

(b) 2D block cyclic distribution of PSelInv sparse matrix data structure on a 4×3 processor grid

Fig. 2. Data layout of the internal sparse matrix data structure used by PSelInv.

Pr × Pc in a cyclic fashion as follows: the $(\mathcal{I}, \mathcal{J})$-th matrix block is held by the processor labeled as

$$P_{\mathrm{mod}(\mathcal{I}-1,\mathrm{Pr})\times\mathrm{Pc}+\mathrm{mod}(\mathcal{J}-1,\mathrm{Pc})+1}. \tag{17}$$

This is called a *2D block cyclic data-to-processor mapping*. The mapping itself does not take the sparsity of the matrix into account. If the $(\mathcal{I}, \mathcal{J})$-th block contains only zero elements, then that block is not stored. It is possible that some nonzero blocks may contain several rows of zeros. These rows are not stored either. As an example, a 4×3 grid of processors is depicted in Figure 2(a). The mapping between the 2D supernode partition of the matrix in Figure 1(a) and the 2D processor grid in Figure 2(a) is depicted in Figure 2(b). Each supernodal block column of L is distributed among processors that belong to a column of the processor grid. Each processor may own multiple matrix blocks. For instance, the nonzero rows in the second supernode are owned by processors P_2 and P_5. More precisely, P_2 owns two nonzero blocks, whereas P_5 is responsible for one block. Note that these nonzero blocks are not necessarily contiguous in the global matrix. Although the nonzero structure of A is not taken into account during the distribution, it has been shown in practice that 2D layouts lead to higher scalability for both dense [Blackford 1997], sparse Cholesky factorizations [Rothberg and Gupta 1994], and LU factorization [Li and Demmel 2003].

In the current implementation, PSelInv contains an interface that is compatible with the SuperLU_DIST software package. To allow PSelInv to be easily integrated with other LDL^T or LU factorization codes, we create some intermediate sparse matrix objects to hold the distributed L and U factors. Such intermediate sparse matrix objects will be overwritten by selected elements of A^{-1} in the selected inversion process. Each nonzero block $L_{\mathcal{I},\mathcal{J}}$ is stored as follows. Diagonal blocks $L_{\mathcal{I},\mathcal{I}}$ are always stored as dense matrices. Nonzero entries of $L_{\mathcal{I},\mathcal{J}}$ $(\mathcal{I} > \mathcal{J})$ are stored contiguously as a dense matrix in a column-major order, even though row indices associated with the stored matrix elements are not required to be contiguous. As mentioned at the beginning of Section 3, our implementation is not optimal in terms of memory allocation for symmetric matrices in the sense that the nonzero entries within $U_{\mathcal{I},\mathcal{J}}$ $(\mathcal{I} < \mathcal{J})$ are also stored as a dense matrix in a contiguous array in a column major order, even

though the values of $U_{\mathcal{I},\mathcal{J}}$ are identical to those of $L^T_{\mathcal{J},\mathcal{I}}$ for symmetric matrices. The nonzero column indices associated with the nonzeros entries in $U_{\mathcal{I},\mathcal{J}}$ are not required to be contiguous either. We remark that for matrices with highly asymmetric sparsity patterns, it is more efficient to store the upper triangular blocks using the skyline structure shown in Li and Demmel [2003]. However, we choose to use a simpler data layout because it allows level-3 BLAS (GEMM) to be used in the selected inversion process.

3.2. Computing Selected Elements of A^{-1} within Each Supernode in Parallel

In this section, we detail how steps 2 through 5 in Algorithm 1 can be completed in parallel.

We perform step 2 of Algorithm 1 in a separate pass, as the data communication required in this step is relatively simple. The processor that owns the block $L_{\mathcal{K},\mathcal{K}}$ broadcasts $L_{\mathcal{K},\mathcal{K}}$ to all other processors within the same column processor group owning nonzero blocks $L_{\mathcal{I},\mathcal{K}}$ in the supernode $\mathcal{K}$. Each processor in that group performs the triangular solve $\hat{L}_{\mathcal{I},\mathcal{K}} \equiv L_{\mathcal{I},\mathcal{K}}(L_{\mathcal{K},\mathcal{K}})^{-1}$ for each nonzero block contained in the set $\mathcal{C}$ defined in step 1 of the algorithm. Because $L_{\mathcal{I},\mathcal{K}}$ is not used in the subsequent steps of selected inversion once $\hat{L}_{\mathcal{I},\mathcal{K}}$ has been computed, it is overwritten by $\hat{L}_{\mathcal{I},\mathcal{K}}$. Since communication is limited to a processor column group only, step 2 can be carried out for multiple supernodes at the same time.

A more complicated communication pattern is required to complete step 3 in parallel. Because $A^{-1}_{\mathcal{C},\mathcal{C}}$ and $\hat{L}_{\mathcal{C},\mathcal{K}}$ are generally owned by different processor groups, there are two possible ways to carry out the multiplication of $A^{-1}_{\mathcal{C},\mathcal{C}}$ with $\hat{L}_{\mathcal{C},\mathcal{K}}$. The first approach is to send blocks of $\hat{L}_{\mathcal{C},\mathcal{K}}$ to processors that own the matching blocks of $A^{-1}_{\mathcal{C},\mathcal{C}}$ so that matrix-matrix multiplication can be performed on processors owning $A^{-1}_{\mathcal{C},\mathcal{C}}$. The second approach is to send data in the opposite direction—that is, one can send blocks of $A^{-1}_{\mathcal{C},\mathcal{C}}$ to the matching blocks of $\hat{L}_{\mathcal{C},\mathcal{K}}$ so that matrix-matrix multiplication can be performed on processors owning $\hat{L}_{\mathcal{C},\mathcal{K}}$.

To compare the cost of these two approaches, let us first consider the case in which all blocks $\hat{L}_{\mathcal{I},\mathcal{K}}$ with $\mathcal{I} \geq \mathcal{K}$ are dense matrix blocks of equal size $m_b \times m_b$, and $\mathcal{C} = \{\mathcal{I} | \mathcal{I} \geq \mathcal{K}\}$. This is approximately the case when $\mathcal{K}$ is near the root of the elimination tree. We assume that there are $\sqrt{P} \times \sqrt{P}$ processors, and thus the size of the set $\mathcal{C}$ is $m_b\sqrt{P}$. We also assume that the matrix blocks in $\hat{L}_{\mathcal{C},\mathcal{K}}$ are distributed among $\sqrt{P}$ processors within the same column group, and each processor in this processor column also holds a dense block $\hat{L}_{\mathcal{I},\mathcal{K}}$ of size $m_b \times m_b$. In the first approach, the computation is performed in parallel on P processors, and the computational cost on each processor is $\mathcal{O}(m_b^3)$. In the second approach, the computation is performed in parallel on $\sqrt{P}$ processors only, and the computational cost on these processors is $\mathcal{O}(m_b^3\sqrt{P})$. All other processors are idle in the computational step, and this leads to severe load imbalance when P is large.

We implemented the first approach in `PSelInv`. This requires sending the $\hat{L}_{\mathcal{I},\mathcal{K}}$ block from a particular processor to all processors within the same column group of processors among which $A^{-1}_{\mathcal{C},\mathcal{I}}$ is distributed. However, since the processor owning $\hat{L}_{\mathcal{I},\mathcal{K}}$ is generally not in the same processor communication group that owns $A^{-1}_{\mathcal{C},\mathcal{I}}$, sending $\hat{L}_{\mathcal{I},\mathcal{K}}$ to processors that hold the distributed blocks of $A^{-1}_{\mathcal{C},\mathcal{I}}$ cannot be done by a single broadcast. Indeed, for this to be possible, communication groups (i.e., MPI communicators) would have to be created for each and every different sparse row/column structure. This is generally not possible, as the maximum number of

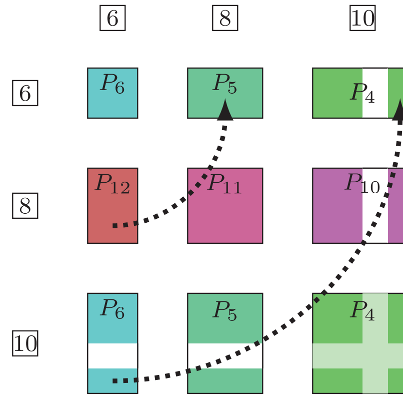

Fig. 3. Processors holding $\hat{L}_{8,6}$ and $\hat{L}_{10,6}$ send data to processors holding the cross-diagonal blocks and overwrite $\hat{U}_{6,8}$ and $\hat{U}_{6,10}$.

allowed MPI communicators is typically much smaller than needed. Therefore, one way to complete this step of data communication is to use a number of point-to-point MPI sends that originate from the processor that owns $\hat{L}_{\mathcal{I},\mathcal{K}}$ and terminate on the group of processors that own the nonzero blocks of $A^{-1}_{\mathcal{C},\mathcal{I}}$. In addition to incurring higher communication latency cost, this approach also leads to significant bookkeeping effort to track the sources and destinations of all messages for each processor.

In our current implementation, we simplify the data communication pattern by storing both $\hat{L}_{\mathcal{I},\mathcal{K}}$ and $\hat{U}_{\mathcal{K},\mathcal{I}}$ even when A is symmetric. We acknowledge that such implementation is not optimal in terms of memory allocation and can be improved if applications are constrained by memory usage for symmetric matrices. As soon as $\hat{L}_{\mathcal{I},\mathcal{K}}$ becomes available as illustrated earlier, we send the $\hat{L}_{\mathcal{I},\mathcal{K}}$ block to the processor that owns $\hat{U}_{\mathcal{K},\mathcal{I}}$, and $\hat{U}_{\mathcal{K},\mathcal{I}}$ is overwritten by $\hat{L}^T_{\mathcal{I},\mathcal{K}}$. Figure 3 illustrates how this step is carried out for a specific supernode $\mathcal{K} = \boxed{6}$ of the matrix described in Figure 2(b). Once $\hat{L}_{8,6}$ is computed on P_{12}, the block is sent to P_5. The P_5 processor then overwrites $\hat{U}_{6,8}$ by $\hat{L}^T_{8,6}$. Similarly, the $\hat{L}_{10,6}$ block is computed on P_6 and sent to P_4, on which $\hat{U}_{6,10}$ is overwritten by $\hat{L}_{10,6}$.

With $\hat{L}_{\mathcal{I},\mathcal{K}}$ properly placed on the processors that are mapped to the upper triangular part of the distributed $\hat{U}$ matrix, step 3 of Algorithm 1 can proceed as follows. The $\hat{U}_{\mathcal{K},\mathcal{I}} = \hat{L}^T_{\mathcal{I},\mathcal{K}}$ block is first sent to all processors within the same column processor group that owns $\hat{U}_{\mathcal{K},\mathcal{I}}$. The matrix-matrix multiplication $A^{-1}_{\mathcal{J},\mathcal{I}}\hat{L}_{\mathcal{I},\mathcal{K}}$ is then performed locally on each processor owning $A^{-1}_{\mathcal{J},\mathcal{I}}$ using the GEMM subroutine in BLAS3. Then local matrix contributions $A^{-1}_{\mathcal{J},\mathcal{I}}\hat{L}_{\mathcal{I},\mathcal{K}}$ are reduced within each row communication groups owning $\hat{L}_{\mathcal{J},\mathcal{K}}$ to produce the $A^{-1}_{\mathcal{J},\mathcal{K}}$ block in step 3 of Algorithm 1.

Figure 4 illustrates how this step is completed for a specific supernode $\mathcal{K} = \boxed{6}$, for the matrix depicted in Figure 2(b). We use circled letters ⓐ, ⓑ, ⓒ to label communication events and circled numbers ①, ②, ③ to label computational events. We can see from this figure that $\hat{U}_{6,8} = \hat{L}^T_{8,6}$ is sent by P_5 to all processors within the same column processor group to which P_5 belongs. This group includes both P_5 and P_{11}. Similarly, $\hat{L}_{10,6}$ is broadcast from P_4 to all other processors within the same column group to which P_4 belongs. Local matrix matrix multiplications are then performed on P_{11}, P_{10}, P_4, and P_5 simultaneously. The distributed products are then reduced onto P_{12} and P_5

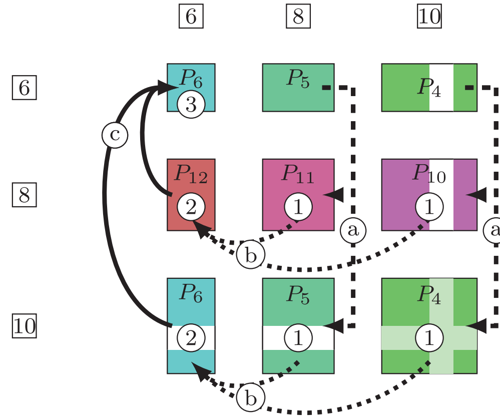

Fig. 4. Task parallelism and communication pattern for the supernode 6. There are six steps: ⓐ broadcast $\hat{L}$, ① compute $A^{-1}\hat{L}$, ⓑ reduce $A^{-1}\hat{L}$, ② compute $\hat{L}^T A^{-1}\hat{L}$, ⓒ reduce $\hat{L}^T A^{-1}\hat{L}$, and ③ update A^{-1}.

respectively within the row processor groups to which they belong. After this step, $A^{-1}_{8,6}$ and $A^{-1}_{10,6}$ respectively become available on P_{12} and P_6.

On completion of step 3, the matrix product $\hat{U}_{\mathcal{K},\mathcal{J}} A^{-1}_{\mathcal{J},\mathcal{K}} \equiv \hat{L}^T_{\mathcal{J},\mathcal{K}} A^{-1}_{\mathcal{J},\mathcal{K}}$ is first computed locally on the processor holding $\hat{L}_{\mathcal{J},\mathcal{K}}$ and then reduced to the processor that owns the diagonal block $L_{\mathcal{K},\mathcal{K}}$ within the column processor group to which the supernode $\mathcal{K}$ is mapped. The sum of the distributed matrix product $-\hat{L}^T_{\mathcal{J},\mathcal{K}} A^{-1}_{\mathcal{J},\mathcal{K}}$ is then added to $(U_{\mathcal{K},\mathcal{K}})^{-1}(L_{\mathcal{K},\mathcal{K}})^{-1}$ computed on the processor holding $L_{\mathcal{K},\mathcal{K}}$. This completes step 4 of Algorithm 1. As an example, again we use Figure 4 for $\mathcal{K} = 6$. $\hat{L}^T_{8,6} A^{-1}_{8,6}$ is computed on P_{12} and sent to P_6. Similarly, $\hat{L}^T_{10,6} A^{-1}_{10,6}$ is computed on P_6. Since both $\hat{L}^T_{10,6}$ and $L_{6,6}$ are held by P_6, no further data communication is necessary. Finally, P_6 updates $A^{-1}_{6,6}$. As we discussed in Section 2.1, for symmetric matrices, $A^{-1}_{\mathcal{K},\mathcal{K}}$ should be explicitly symmetrized to reduce the effect of rounding errors.

Since A is symmetric, dtep 5 of Algorithm 1 can be simplified as follows. We first overwrite $\hat{L}_{\mathcal{J},\mathcal{K}}$ by $A^{-1}_{\mathcal{J},\mathcal{K}}$ locally on the processor holding $\hat{L}_{\mathcal{J},\mathcal{K}}$ ($\mathcal{J} > \mathcal{K}$). We then send $A^{-1}_{\mathcal{J},\mathcal{K}}$ to the processor holding $\hat{U}_{\mathcal{K},\mathcal{J}}$ and overwrite $\hat{U}_{\mathcal{K},\mathcal{J}}$ by $(A^{-1}_{\mathcal{J},\mathcal{K}})^T$. The data communication pattern for this step is the same as described in Figure 3. After step 5, we move to the next supernode ($\mathcal{K} - 1$).

3.3. Exploiting Concurrency in the Elimination Tree

In this section, we discuss how to add an additional coarse-grain level of parallelism to the selected inversion algorithm by exploiting task concurrency exposed by the elimination tree.

As we indicated in Section 2.2, two supernodes belonging to two separate branches of the elimination tree can be processed independently if the selected elements of the inverse belonging to their ancestors have been computed, and if these supernodes and the ancestors on which they depend are mapped onto different sets of processors. Although it is possible to pass the previously computed selected elements of A^{-1} from the ancestors down to their children as we move down the elimination tree, algorithms based on this approach (e.g., a multifrontal like algorithm [Lin et al. 2011a]) would require additional work space to hold extra copies of the selected elements.

To reduce the amount of extra work space, which can grow rapidly as we go down the elimination tree, we choose to allow processors assigned to each supernode to communicate back and forth with processors assigned to its ancestors in the way that we described in Section 3.2 to complete step 3 of Algorithm 1.

However, the drawback of this approach is that at some point, two supernodes belonging to two separate branches of the elimination tree may not be processed simultaneously when they need to communicate with their common ancestors at the same time. At this point of conflict, only one of them should be allowed to initiate and complete the data communication with the common ancestor at a time. For example, when supernodes 2 and 4 in Figure 1(a) are being processed on different sets of processors, both of them may need to communicate with processors assigned to supernode 5 at the same time. In this case, the updates to be performed on these processors cannot proceed completely independently. On the other hand, if the set of processors assigned to update two supernodes are completely different, then at least some of the updates can be computed simultaneously.

To exploit the type of concurrency discussed previously, which occurs at the `for` loop level in Algorithm 1, we create a basic parallel task scheduler to launch different iterates of the `for` loop in a certain order. This order is defined by a priority list S, which is indexed by integer priority numbers ranging from 1 to n_s, where n_s is bounded from above by the depth of the elimination tree. The task performed in each iteration of the `for` loop is assigned a priority number $\sigma(\mathcal{I})$. The lower the number, the higher the priority of the task, and hence the sooner it is scheduled. The supernode $\mathcal{N}$ associated with the root of the elimination tree clearly has to be processed first. If the k-th element of S contains multiple supernodes or tasks whose priority numbers are k, the order in which these tasks are completed can be arbitrary. A recipe for assigning priority number of different tasks (or equivalently, supernodes) is shown in Algorithm 2. We assume that the elimination tree is post ordered.

Even though we use a priority list to help launch tasks, we do not place extra synchronization among launched tasks other than requiring them to preserve data dependency. Tasks associated with different supernodes can be executed concurrently if these supernodes are on different critical paths of the elimination tree, and if there is no overlap among processors mapped to these critical paths. In fact, if tasks associated with supernode $\mathcal{J}$ and $\mathcal{I}$ are mapped to different sets of processors, the task associated with the supernode $\mathcal{J}$ may actually start before that associated with another supernode $\mathcal{I}$ even if $\sigma(\mathcal{I}) < \sigma(\mathcal{J})$—that is, even if task $\mathcal{I}$ is scheduled ahead of task $\mathcal{J}$ according to the priority list. When two different tasks need to communicate with a common ancestor, the priority number associated with each task determines which task is completed first.

ALGORITHM 2: Assign Priority Numbers to Supernodes and Create a Priority List.

Input: A list of supernodes $\{\mathcal{I}\}$ and the elimination tree associated with these supernodes.
Output: An array σ, $\sigma(\mathcal{I})$ gives the priority number of the task associated with supernode $\mathcal{I}$; an array S of n_s supernode lists, $S(i)$ gives a set of supernodes with priority number i, $1 \le i \le n_s$.

Q5

$\sigma(\mathcal{N}) = 1$
$S(1) = \{\mathcal{N}\}$
for $\mathcal{I} = \mathcal{N} - 1$ *down to* 1 **do**
  $\sigma(\mathcal{I}) = \sigma(\text{parent}(\mathcal{I})) + 1$
  $S(\sigma(\mathcal{I})) = S(\sigma(\mathcal{I})) \cup \{\mathcal{I}\}$
end

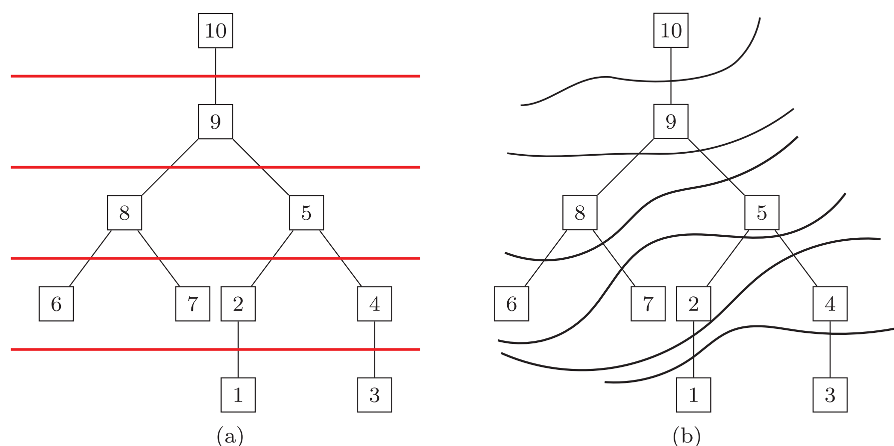

Fig. 5. Elimination tree of matrix A and two possible priority lists S.

We remark that there is some flexibility in assigning a priority number to each supernode and constructing the priority list S. For instance, we can use the strategy given by Algorithm 2, which simply defines $\sigma(\mathcal{I})$ by the distance (in terms of the number of edges) between the supernode $\mathcal{I}$ and the root of the elimination tree. For the same elimination tree shown in Figure 5(a), another possible construction of the σ list is illustrated in Figure 5(b), which assigns the same σ value to supernodes at different levels of the elimination tree. The latter construction takes into account how supernodes are distributed among different processors, as we will discuss in the following.

The priority list S determines the order in which computational tasks associated with different supernodes are completed. Because the amount of work and communication performed by each of the supernodes can vary significantly, different priority lists can lead to different overall performance. The actual performance of parallel selected inversion depends on the sparsity pattern of the matrix, as well as the processor grid, and is therefore difficult to predict a priori. We refer readers to our report [Jacquelin et al. 2014] for a detailed example on the difficulty of designing an optimal task schedule.

With the help of the priority list, we can implement the `for` loop level of parallelism in Algorithm 1 in a way that is described in Algorithm 3. To illustrate the relation clearly, Algorithm 3 uses the same numeric ordering of the steps as that in Algorithm 1. Algorithm 3 also makes use of another array of lists `procmap`. The $\mathcal{K}$-th element of `procmap` contains the list of all processors participating in steps 3 through 5 in Algorithm 1. The communication steps are described within parentheses. We also remark that we do not place MPI barriers between supernodes explicitly to exploit parallelism among the computation for different supernodes. For symmetric matrices, the diagonal blocks should be symmetrized, as indicated at the end of Section 2.1 for symmetric cases.

4. NUMERICAL RESULTS

To assess the performance of `PSelInv`, we conducted several computational experiments, which we report in this section.

Our test problems are taken from various sources, including the Harwell-Boeing Test Collection [Duff et al. 1992] and the University of Florida Matrix Collection [Davis and Hu 2011], and matrices generated from electronic structure software, including SIESTA [Soler et al. 2002] and DGDFT [Lin et al. 2012]. The first two matrix collections are widely used benchmark problems for testing sparse direct methods, whereas the other test problems come from practical large-scale electronic structure

ALGORITHM 3: The Parallel Selected Inversion Algorithm (for Symmetric Matrices).

Input: (1) The supernode partition of columns of a sparse symmetric matrix A: $\{1, 2, \ldots, \mathcal{N}\}$; a priority list $\{S(k)\}$: $k = 1, 2, \ldots, n_s$;
(2) L and U factors through a supernodal LU factorization (or equivalent LDL^T factorization) of A;
(3) 2D processor mapping with with $P = \mathrm{Pr} \times \mathrm{Pc}$ processors.

Output: Selected elements of A^{-1}.

```
[Compute the normalized factors L̂ and Û].
for k = 1, 2,..., n_s do
    for each supernode K ∈ S(k) do
        if myid ∈ procmap(K) then
1           Find the collection of indices
            C = {I | I > K, L_{I,K} is a nonzero block} ∪ {J | J > K, U_{K,J} is a nonzero block}
2           (Broadcast (L_{K,K})^{-1} to processors owning L_{I,K}, I ∈ C)
2           L̂_{C,K} ← L_{C,K}(L_{K,K})^{-1}
2           (Send L̂_{I,K}, I ∈ C to the processor holding Û_{K,I}, I ∈ C and overwrite Û_{K,I}, I ∈ C
              by L̂^T_{I,K}, I ∈ C)
        end
    end
end
[Selected inversion process].
for k = 1, 2,..., n_s do
    for each supernode K ∈ S(k) do
        if myid ∈ procmap(K) then
            Find the collection of indices
            C = {I | I > K, L_{I,K} is a nonzero block} ∪ {J | J > K, U_{K,J} is a nonzero block}
3           (Broadcast Û_{K,I}, I ∈ C to processors holding A^{-1}_{J,I}, I, J ∈ C)
3           For processors holding A^{-1}_{J,I}, I, J ∈ C, compute locally −A^{-1}_{J,I} L̂_{I,K}, I, J ∈ C
3           (Reduce −A^{-1}_{J,I} L̂_{I,K}, I, J ∈ C to processors holding L̂_{J,K}, J ∈ C, and save the
            result in A^{-1}_{J,K}, J ∈ C)
4           For processors holding L̂_{I,K}, I ∈ C, compute locally −L̂^T_{I,K} A^{-1}_{I,K}, I ∈ C
4           (Reduce −L̂^T_{I,K} A^{-1}_{I,K}, I ∈ C to the processor holding L_{K,K})
4           For the processor holding (L_{K,K})^{-1}, update A^{-1}_{K,K} ← (U_{K,K})^{-1}(L_{K,K})^{-1} − L̂^T_{C,K} A^{-1}_{C,K}
            For the processors holding L^{-1}_{K,K}, update A^{-1}_{K,K} ← 1/2 (A^{-1}_{K,K} + A^{-T}_{K,K})
3           Overwrite L̂_{I,K}, I ∈ C by A^{-1}_{I,K}, I ∈ C
5           (Send A^{-1}_{I,K}, I ∈ C to the processor holding Û_{K,I}, I ∈ C, and overwrite Û_{K,I}, I ∈ C
            by A^{-1}_{I,K}, I ∈ C)
        end
    end
end
```

calculations. The names of these matrices, as well as some of their characteristics, are listed in Tables I and II. The first three problems in these tables come with two matrices each. One of the matrices, denoted by H, is a discretized Hamiltonian, and the other matrix is an overlap matrix, denoted by S. For all other problems, the overlap matrices can be considered as the identity matrix. All matrices are real and symmetric. In all of our experiments, we compute the selected elements of the matrix

$$A(z) = H - zS. \tag{18}$$

Table I. Description of Test Problems for PSelInv

Problem	Description
SIESTA_C_BN_1x1	Electronic structure theory, C-BN sheet with 2,532 atoms
SIESTA_C_BN_2x2	Electronic structure theory, C-BN sheet with 10,128 atoms
SIESTA_C_BN_4x2	Electronic structure theory, C-BN sheet with 20,256 atoms
DNA_16	Electronic structure theory, DNA molecule with 11,440 atoms
DNA_715_64cell	Electronic structure theory, DNA molecule with 45,760 atoms
DG_Graphene_2048	Electronic structure theory, graphene with 2,048 atoms
DG_Graphene_8192	Electronic structure theory, graphene with 8,192 atoms
pwtk	Pressurized wind tunnel, stiffness matrix
parabolic_fem	Diffusion-convection reaction, constant homogeneous diffusion
ecology2	Circuitscape: circuit theory applied to animal/gene flow, B. McRae, UCSB
audikw_1	Automotive crankshaft model with more than 900,000 TETRA elements, Audi, GmbH

Table II. Dimension n, the Number of Nonzeros $|A|$, and the Number of Nonzeros of the Cholesky Factor $|L|$ of the Test Problems

Problem	n	$\|A\|$	$\|L\|$
SIESTA_C_BN_1x1	32,916	23,857,418	269,760,112
SIESTA_C_BN_2x2	131,664	95,429,672	1,655,233,542
SIESTA_C_BN_4x2	263,328	190,859,344	3,591,750,262
DNA_16	7,752	2,430,642	9,272,160
DNA_715_64cell	459,712	224,055,744	866,511,698
DG_Graphene_2048	82,944	87,340,032	545,245,344
DG_Graphene_8192	331,776	349,360,128	2,973,952,468
pwtk	217,918	5,926,171	104,644,472
parabolic_fem	525,825	3,674,625	58,028,731
ecology2	999,999	2,997,995	91,073,583
audikw_1	943,695	77,651,847	2,500,489,909

For simplicity, we choose $z = 0$ for all efficiency tests in Section 4.1. For some applications, z is chosen to be a complex number with a small imaginary part to ensure that $A(z)$ is nonsingular. This technique is often used in the electronic structure calculation to be discussed in Section 4.3. The LU factorization is performed by using the SuperLU_DIST software package. SuperLU_DIST does not use dynamic pivoting strategies, and our matrices are permuted without taking into account the values of matrix entries. Consequently, the efficiency of both SuperLU_DIST and PSelInv is independent of the choice of z. The lack of dynamic pivoting strategies may impact the accuracy of PSelInv for highly indefinite and nearly singular systems. We study the accuracy for different choices of complex shifts z in Section 4.2. All timing results reported are performed in complex arithmetic computation.

In all of our experiments, we used the NERSC Edison platform with Cray XC30 nodes. Each node has 24 cores partitioned among two Intel Ivy Bridge processors. Each 12-core processor runs at 2.4GHz. A single node has 64GB of memory, providing more than 2.6GB of memory per core. We used one MPI process per core and refer to the core to denote an MPI process.

4.1. Parallelization Scalability

Four types of experiments were performed to measure the scalability of PSelInv. For the first three sets of experiments, all timing data points that we present are averaged measurements over 10 runs, and the error bars shown in Figures 6, 7, 8, and 9 indicate the standard deviation of the measured wall clock time.

To clearly show the cost and scalability of selected inversion itself in comparison with the symbolic and numerical LU factorizations, which are required for selected

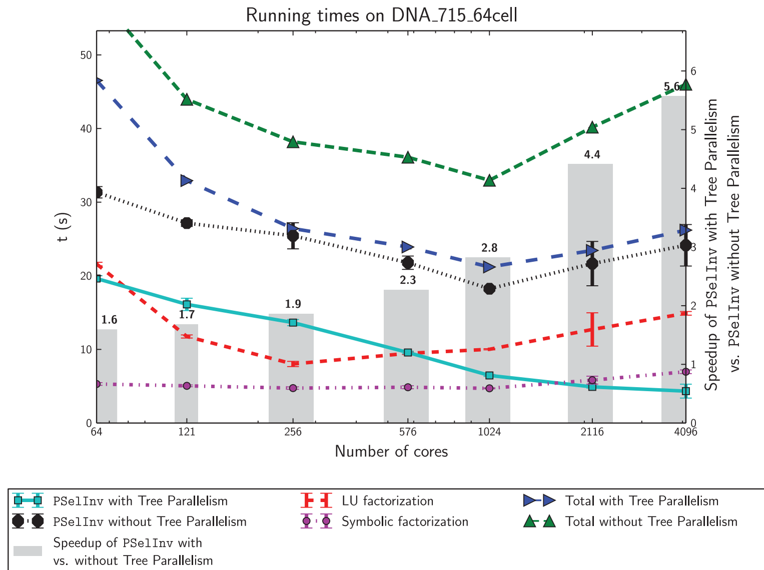

Fig. 6. Wall clock time used by three components (symbolic factorization, numerical LU factorization, and selected inversion) of two versions of PSelInv with respect to the number of cores used in the computation for the DNA_715_64cell matrix. In one version, we do not take advantage of the concurrency exposed by the elimination tree, whereas in the other version, we do make use of this tree level of parallelism. The height of each bar in the figure indicates the ratio of wall clock time measured for the former over that measured for the latter.

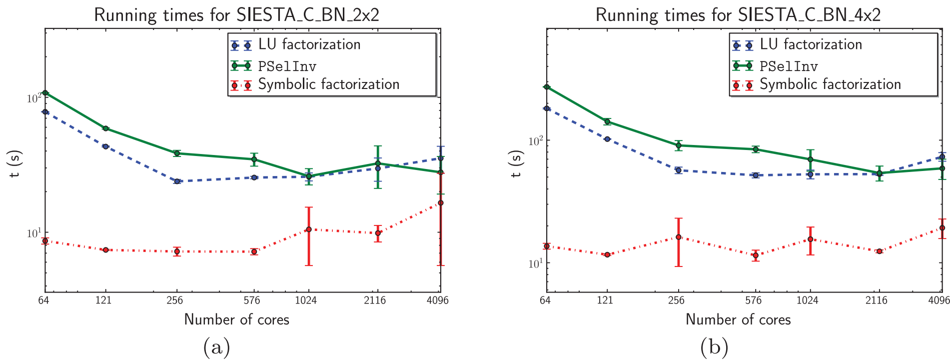

Fig. 7. Strong scalability of PSelInv compared to that of LU factorization and symbolic factorization for SIESTA matrices generated for two C_BN systems of different sizes.

inversion, we time the three computational components separately. The symbolic factorization is performed in parallel using PT-Scotch. It is labeled as "symbolic factorization" in the timing figures. The LU factorization is performed by using SuperLU_DIST. It is labeled as "LU factorization." The selected inversion itself is performed by using PSelInv and labeled as "PSelInv." The total time required to obtain the selected elements of the inverse matrix thus corresponds to the sum of all three components.

The first experiment focuses on the impact of the additional parallelism stemming from the elimination tree as discussed in Section 3.3. PSelInv is thus tested both with and without this additional level of parallelism. As observed in Figure 6, adding the tree-level parallelism allows the performance of PSelInv to scale to 4,096 cores. When

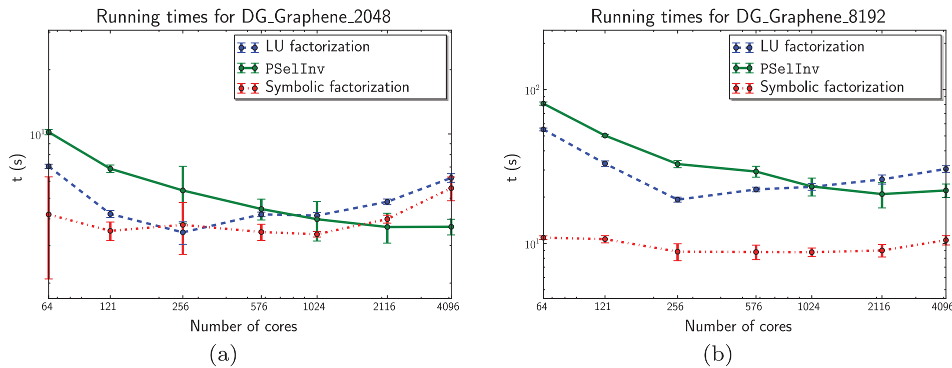

Fig. 8. Strong scalability of PSelInv compared to that of LU factorization and symbolic factorization for DG matrices generated for graphene systems of different sizes.

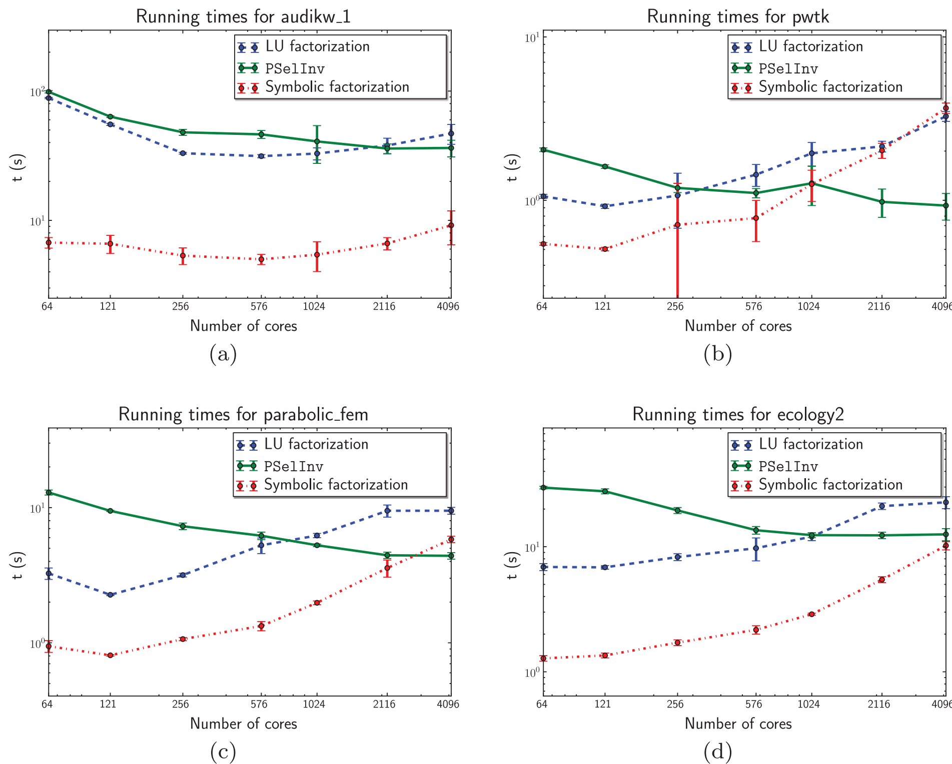

Fig. 9. Strong scalability of PSelInv compared to that of LU factorization and symbolic factorization for matrices from the Harwell-Boeing Test Collection and the University of Florida Matrix Collection.

4,096 cores are used, adding the tree-level parallelism leads to a 5.6-fold speedup in the DNA_715_64cell problem. Comparatively, the performance of the LU factorization and the selected inversion without tree parallelism can only scale up to 1,024 cores.

The second set of experiments (Figures 7, 8, and 9) aims at evaluating the strong scaling of PSelInv. In every experiment, the tree-level parallelism is enabled, as it clearly delivers better performance. PSelInv exhibits excellent strong scalability up to

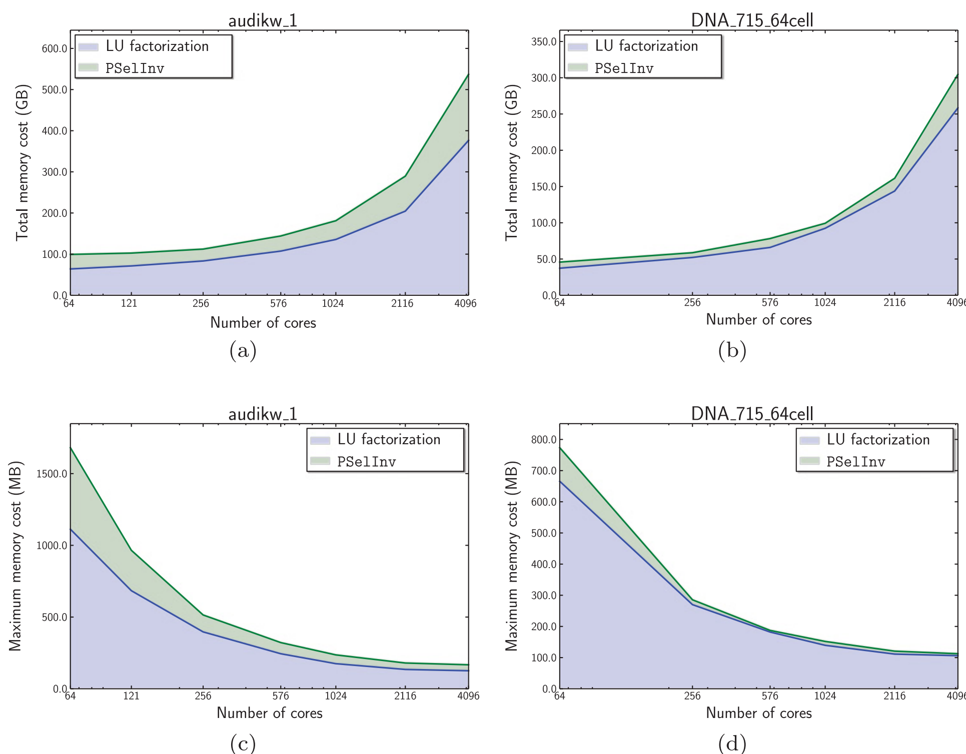

Fig. 10. Cumulative total memory cost and maximum memory cost among all cores for the audikw_1 matrix and the DNA_715_64cell matrix, with shaded regions indicating the additional memory cost introduced in each step of the selected inversion process. The memory cost is measured by the memory high watermark reached at each step.

4,096 cores. For SIESTA matrices (Figure 7), PSelInv is slightly slower than LU factorization when the number of cores is less than 1,024 and is faster than LU factorization when more than 2,116 cores are used. For DGDFT matrices (Figure 8), PSelInv can be twice as fast as LU factorization, and the running time of PSelInv can be comparable to that of symbolic factorization for the DNA_715_64cell matrix. For generic sparse matrices (Figure 9) obtained from the University of Florida Collection, PSelInv delivers excellent performance on relatively dense matrices, such as audikw_1 and pwtk. We also observe that for highly sparse problems, such as ecology_2 and parabolic_fem, PSelInv is relatively more costly, but the scalability of PSelInv can still be better than that of SuperLU_DIST when a large number of cores are used.

The third experiment focuses on the memory cost of PSelInv. Figure 10 shows the cumulative total memory cost and cumulative maximum single-core memory usage in the parallel selected inversion procedure for two matrices: audikw_1 and DNA_715_64cell. This is measured by the memory high watermark reached after the LU factorization step and the selected inversion step, respectively. The memory cost for reading the input matrix is much smaller compared to the memory cost of LU factorization or selected inversion. The shaded areas in Figure 10 correspond to the additional memory required to perform each step of the procedure. The memory high watermark implies that the memory cost for LU factorization includes not only the memory cost for the LU factors but also other temporary memory allocation created during the LU factorization process. The situation is similar for the selected inversion process. The memory

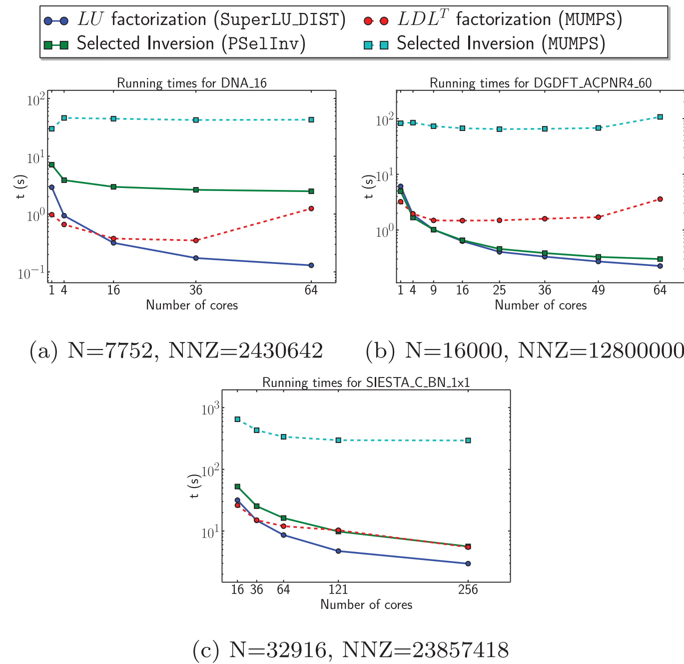

(a) N=7752, NNZ=2430642 (b) N=16000, NNZ=12800000

(c) N=32916, NNZ=23857418

Fig. 11. Performance comparison against MUMPS 4.10.0 for computing selected elements of the inverse.

required to store both the LU factors and the corresponding elements in the inverse is lower than the overall memory high watermark, which accounts for additional memory required to hold communication and temporary buffers. We can see from Figure 10 that most of the memory allocation is done during the LU factorization step. The total memory cost of LU factorization and selected inversion increases as the number of cores increases due to the use of additional buffer arrays for communication and computation.

The total additional memory cost of PSelInv is 20% to 60% of the total memory required by LU factorization, which is relatively small. The maximum memory usage per core decreases steadily as the number of cores increases. For our test problems, the maximum memory cost per core of PSelInv is around 1GB when a relatively small number (64) of cores are used. It decreases to around 100MB when a large number (4,096) of cores are used for the same problem.

The last set of experiments compare the performance of PSelInv to the parallel matrix inversion method recently implemented in the MUMPS package [Amestoy et al. 2012a]. In the MUMPS algorithm, the actual set of computed entries of A^{-1} is also a superset of the requested entries of A^{-1}. This method can be more efficient than PSelInv when a small number of entries of A^{-1} are requested. However, when a relatively large number of entries are to be computed, such as in the computation of the selected elements defined by (1), PSelInv can more efficiently reuse the information shared among different entries of A^{-1}. Figure 11 shows the numerical factorization and selected inversion timings for MUMPS and PSelInv, respectively. As all matrices are symmetric, MUMPS performs LDL^T factorizations, which use fewer floating point operations and less memory. We use MUMPS to compute the selected elements of A^{-1} as defined in Equation (1) for DNA_16 and SIESTA_C_BN_1x1, and we also use MUMPS to only compute the diagonal entries of A^{-1} for DGDFT_ACPNR4_60. All three matrices

Table III. Comparison of Wall Clock Time Required by PSelInv and MUMPS for Computing the Selected Elements Defined by (1) of Two Matrices DNA_16 and SIESTA_C_BN_1x1, and the Diagonal Elements of DGDFT_ACPNR4_60

Problem	Cores (#)	PSelInv	MUMPS
DNA_16	1	3.1	29.9
DNA_16	16	2.9	44.6
DGDFT_ACPNR4_60	1	4.9	82.6
DGDFT_ACPNR4_60	16	0.6	67.1
SIESTA_C_BN_1x1	16	52.6	648.2
SIESTA_C_BN_1x1	256	5.6	293.7

come from electronic structure applications, and the difference in terms of computed entries is determined by the different requirements in practical calculations. MUMPS contains a block size parameter that controls the number of right-hand sides processed simultaneously. We experimented with this parameter and report the best results that we could produce for each case (i.e., 16 for DNA_16 and 256 for SIESTA_C_BN_1x1 and DGDFT_ACPNR4_60). Table III shows how the wall clock time used by PSelInv compares to that used by MUMPS for three test problems: DNA_16, DGDFT_ACPNR4_60, and SIESTA_C_BN_1x1.

For all test problems, PSelInv is at least an order of magnitude faster than MUMPS. It is two orders of magnitude faster on SIESTA_C_BN_1x1 when using 256 cores. PSelInv can also scale to a relatively larger number of cores. Our numerical results indicate that for the computation of selected elements as considered in this article, PSelInv is more efficient than the more general approach taken in MUMPS.

One way to understand the speedup of PSelInv over MUMPS is through the following idealized situation. Consider the computation of the diagonal entries of a tridiagonal matrix A of size N, which can be computed by solving an N set of triangular equations of the form (5). Even with the help of the elimination tree and the fact that only one entry of A^{-1} is needed for each equation, the cost for solving all N equations independently would be $\mathcal{O}(N^2)$. The reason for the high computational cost is that a significant amount of information calculated among the N equations is redundant. The MUMPS approach detects such redundant information on the fly through graph-based algorithms. However, designing an optimal algorithm that maximally reduces the amount of redundant information for a given data-to-processor mapping is difficult. The resulting implementation may or may not reach the optimal complexity. In contrast, PSelInv removes all redundant calculation by design, and the computational cost for a tridiagonal matrix can be provably reduced to $\mathcal{O}(N)$ [Lin et al. 2009b].

We should point out that MUMPS can compute an arbitrary set of elements of A^{-1}, whereas the set of selected elements that can be computed by PSelInv is more restrictive, as defined in Equation (1).

Overall, the strong scalability of PSelInv is similar to that of SuperLU_DIST, and it clearly outperforms the current inversion algorithm as implemented in MUMPS. It requires a modest amount of additional memory to compute the selected elements of the inverse. This observation demonstrates both the validity of our approach and the efficiency of our implementation. More importantly, on matrices arising from actual electronic calculations, PSelInv allows one to use thousands of cores, thereby enabling very large scale computations.

4.2. The Accuracy of PSelInv

In exact arithmetic, the selected inversion method is an exact method for computing the selected elements of A^{-1}, regardless of whether A is positive definite or not. In practice, the selected inversion method cannot give an exact result due to the presence of

Table IV. Maximum Column-Wise Relative Error between MUMPS and PSelInv Using Different Numbers of Cores *P*

P	Max. Relative Error
1	8.52E-008
4	2.35E-008
16	2.52E-008
36	2.05E-007
64	2.07E-007

(a) DNA_16

P	Max. Relative Error
16	1.96E-007
36	1.72E-007
64	1.77E-007
121	1.76E-007
256	1.78E-007

(b) SIESTA_C_BN_1x1

642 round-off errors. For the sparse direct solver, dynamical pivoting strategies such as the
643 Bunch-Kaufman process [Bunch and Kaufman 1977] for LDL^T factorization has been
644 shown to be effective for reducing the numerical error, especially for indefinite matri-
645 ces. On distributed memory machines, dynamic pivoting strategies can significantly
646 affect the load balance and the scalability of the factorization process. Thus, they are
647 not used in `SuperLU_DIST` [Li and Demmel 2003].

648 Since the primary goal of the current implementation of the `PSelInv` method is to
649 achieve high parallel scalability, we choose not to perform additional pivoting steps
650 after the factorization step. We show that for the test problems we tried, `PSelInv`
651 produces results comparable to that produced by the `MUMPS` package and is sufficiently
652 accurate even when the matrix is relatively ill conditioned.

653 The first set of experiments report comparative results between `MUMPS` and
654 `PSelInv` on two problems benchmarked in Section 4.1. Selected elements are com-
655 puted with both methods, and their maximum relative column-wise difference
656 $\max_{1\le j\le n}(\|A^{-1}_{\mathtt{MUMPS}_{*,j}} - A^{-1}_{\mathtt{PSelInv}_{*,j}}\|/\|A^{-1}_{\mathtt{MUMPS}_{*,j}}\|)$ is presented in Table IV. In both cases,
657 `PSelInv` provides accurate results that are comparable to `MUMPS` on these two problems.

658 In the second set of experiments, we assess the accuracy of `PSelInv` on larger ill-
659 conditioned matrices. To obtain test problems that are indefinite and ill conditioned,
660 for each test problem listed in Table II, we construct a sequence of $A(z)$ defined by
661 Equation (18) for several complex shifts z. The real parts of the shifts lie within the
662 spectrum of the matrix pencil (H, S), and the imaginary parts range from small (10^{-7})
663 to large (10^{-1}) values.

664 To quantify the accuracy of the `PSelInv` method for large matrices in the test set,
665 we need to find an appropriate error metric. Due to the large matrix size, the parallel
666 matrix inversion method in `MUMPS` becomes too expensive to be used for the purpose of
667 benchmarking. Motivated by the trace estimation in Equation (2), we choose to measure
668 the numerical error introduced by `PSelInv` by using the following quantity:

$$E(z) = \frac{|N - \mathrm{Tr}[A(z)^{-1}A(z)]|}{N} \equiv \left|1 - \frac{1}{N}\sum_{i,j=1}^{N}[A(z)^{-1}]_{ij}[A(z)]_{ji}\right|. \qquad (19)$$

669 Since A is sparse, the summation in Equation (19) involves only those i and j such that
670 $A_{i,j} \neq 0$.

671 In Figure 12, we show both the spectral density $\rho(\lambda)$ of the pwtk matrix, which
672 describes the number of eigenvalues of eigenvalues (H, S) per unit interval, and $E(z)$
673 for several shifts z with different real and imaginary parts. We observe that for all of
674 these problems, the measured errors are below 10^{-11}, even when the real part of z is
675 close to an eigenvalue cluster and the imaginary part of z is as small as 10^{-7}. Figure 13
676 shows that a similar level of accuracy is achieved in the test of the DNA_715_64cell
677 matrix.

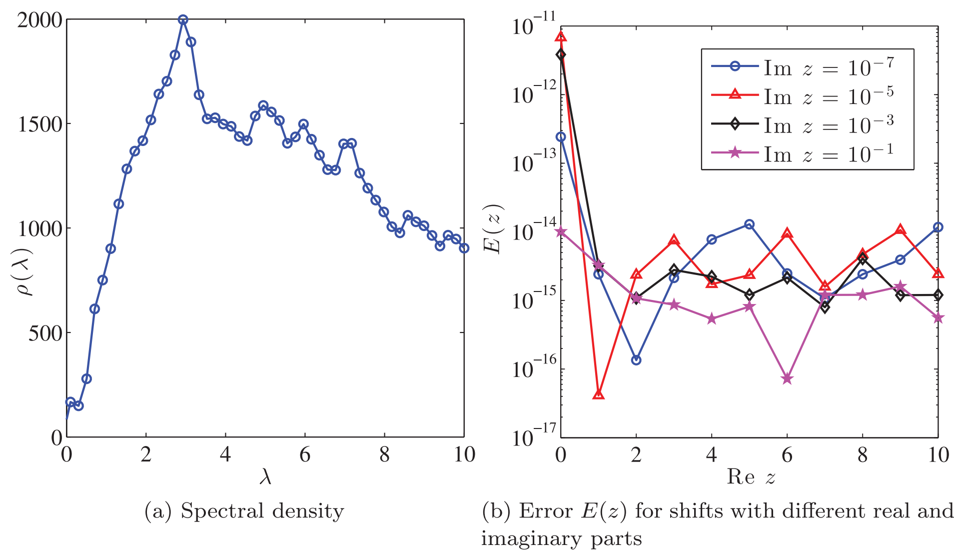

(a) Spectral density

(b) Error $E(z)$ for shifts with different real and imaginary parts

Fig. 12. Spectral density and error $E(z)$ for the pwtk matrix.

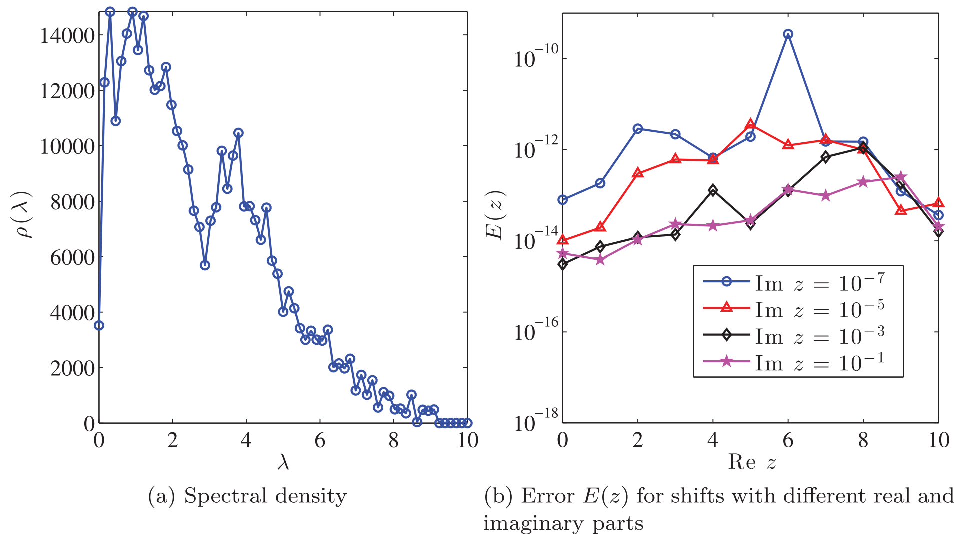

(a) Spectral density

(b) Error $E(z)$ for shifts with different real and imaginary parts

Fig. 13. Spectral density and error $E(z)$ for the DNA_715_64cell matrix.

4.3. Application to Electronic Structure Theory

In this section, we demonstrate how PSelInv can be applied to accelerate Kohn-Sham density functional theory (KSDFT) calculation [Hohenberg and Kohn 1964; Kohn and Sham 1965], which is widely used for describing the ground state electronic properties of molecules, solids, and other nanostructures. We use the recently developed pole expansion and selected inversion technique (PEXSI) [Lin et al. 2009a, 2009b, 2011b, 2013] to compute the nonzero elements of the so-called single particle density matrix

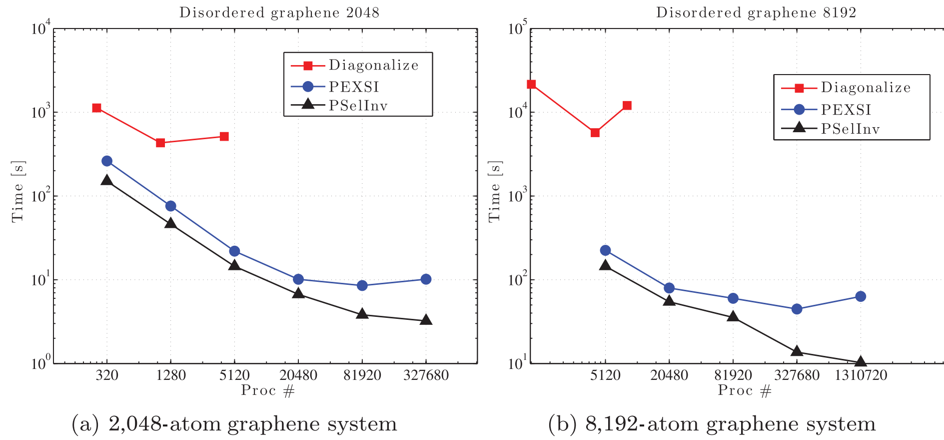

(a) 2,048-atom graphene system

(b) 8,192-atom graphene system

Fig. 14. Wall clock time versus the number of cores for a graphene system.

Γ that can be approximated by

$$\Gamma \approx \sum_{l=1}^{P} \omega_l (H - z_l S)^{-1}, \tag{20}$$

where $z_l, \omega_l \in \mathbb{C}$, and the number of "poles" P is around 80 in practical calculations. Both H and S are real sparse symmetric matrices that have the same sparsity pattern when a local basis set is used to discretize the Kohn-Sham problem. Each matrix $A_l = H - z_l S$ is a complex symmetric matrix. In KSDFT calculations, only elements of Γ_{ij} corresponding to the nonzero elements of H and S (i.e., $H_{ij}, S_{ij} \neq 0$) are needed to compute physical quantities such as electron density and energy. The expansion (20) immediately suggests that only the selected elements as defined in Equation (1) of the matrices A_l^{-1} are needed. In a parallel implementation of PEXSI, we use `PSelInv` to evaluate the selected elements of A_l^{-1} that correspond to the nonzero elements of Γ on a subset of cores. The selected inversion of A_l for different l can be carried out independently on different subsets of cores.

We apply the parallel PEXSI method to the DG_Graphene_2048 and DG_Graphene_8192 systems, which are disordered graphene systems with 2,048 and 8,192 atoms, respectively, and compare its performance to a standard approach that requires a partial diagonalization of (H, S). We use a ScaLAPACK subroutine pdsyevr [Vömel 2010], which is based on the multiple relatively robust representations (MRRR) algorithm, to perform such diagonalization. Although both H and S are sparse matrices, the MRRR algorithm treats them as dense matrices. For $H, S \in \mathbb{R}^{N \times N}$, the MRRR algorithm first performs a tridiagonalization procedure with $\mathcal{O}(N^3)$ cost, then efficiently solves the eigenvalues and eigenvectors of the tridiagonal system with $\mathcal{O}(N^2)$ cost, and finally the eigenvectors can be constructed with $\mathcal{O}(N^3)$ cost.

Figure 14(a) shows that the scalability of pdsyevr is limited to 1,024 cores for the 2,048-atom problem. Adding more cores to the diagonalization process leads to an increase of the wall clock time due to communication overhead. For this relatively small problem, the benefit of parallel implementation of PEXSI is already clear when 320 cores are used. Since we use $P = 80$ poles in the pole expansion, 4 cores with a 2×2 processor grid are used in each selected inversion in this case. The wall clock time used by PEXSI is 261 seconds, among which 150 seconds are attributed to `PSelInv`, 95 seconds are attributed to factorization, and 10 seconds are attributed to symbolic

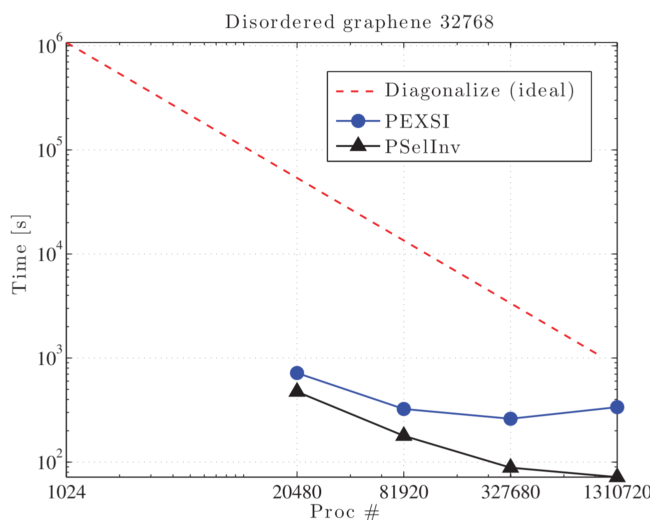

Fig. 15. Wall clock time versus the number of cores for a graphene system with 32,768 atoms.

factorization. This timing result compares favorably to the 430 seconds of measured wall clock time required by pdsyevr on 1,024 cores.

Furthermore, we can clearly see from Figure 14(a) that the parallel PEXSI method can scale to a much larger number of cores. Nearly perfect speedup can be observed when a total of 20,480 cores is used in the parallel PEXSI computation, with 256 cores used in each selected inversion. The total wall clock time used in this calculation is merely 10 seconds. Compared to the best wall clock time that we can obtain for the diagonalization procedure, which is 430 seconds on 1,024 cores, this represents a speedup factor of 43.

For the larger system that contains 8,192 atoms, pdsyevr can scale to 4,096 cores, as we can see in Figure 14(b). It takes 5,703 wall clock seconds to perform such a computation. When the parallel PEXSI calculation is carried out on 5,120 cores with 64 cores used to perform each selected inversion, the total wall clock time required is 224 seconds. Figure 14(b) also shows that parallel PEXSI can scale to as many as 327,680 cores with 4,096 cores used for each selected inversion. The total wall clock time required in this calculation is merely 45 seconds, a 127-fold speedup compared to the best diagonalization wall clock time measured.

Finally, we apply PEXSI to a system with 32,768 atoms. The matrix size is four times larger than that for the system with 8,192 atoms, and the diagonalization routine is no longer feasible: the wall clock time required to run the pdsyevr routine with 1,024 cores for the 2,048-atom system is 431 seconds, and for the 8,192-atom system, it is 21,556 seconds. The increase of the wall clock time is 50 fold, which is roughly in agreement with the cubic complexity scaling factor $4^3 = 64$. The cubic scaling of the diagonalization procedure implies that the wall clock time would increase by at least a factor of 50 to 1,077,800 seconds (300 hours) if we perform the same type of calculation for a system that contains 32,768 atoms on 1,024 cores. Based on this estimation and assuming that the strong scaling of pdsyevr is perfect, we compare the ideal performance of the diagonalization method to the practical performance of PEXSI in Figure 15 up to 1,310,720 cores. The total wall clock time for both factorization and selected inversion reaches its minimum at 4,096 cores per pole (327,680 cores in total), which is 241 seconds. Among these, 87 seconds is attributed to PSelInv. Comparatively, even if the diagonalization procedure scales perfectly to more than one million cores,

747 which is highly unlikely within the current framework of diagonalization methods, the
748 projected wall clock time is greater than 1,000 seconds, which is significantly more
749 than that used by PEXSI.

750 5. CONCLUSIONS AND FUTURE WORK

751 We described an efficient parallel implementation of the selected inversion algorithm
752 for distributed memory parallel machines. The current implementation of `PSelInv` can
753 be applied to the computation of selected elements of the inverse of a sparse symmetric
754 matrix. It is publicly available and can scale to more than 4,000 cores for sufficiently
755 large problems. The scalability of the solver depends on the size and sparsity of the
756 matrix. We observed that it is important to exploit concurrency available within the
757 elimination trees to achieve high scalability in the parallel selected inversion process.
758 In the future, we plan to further improve the tree-level parallelism to enhance the con-
759 currency among different supernodes. We also observed that for our test problems, the
760 `PSelInv` method is relatively accurate even for matrices that are highly indefinite and
761 close to singular. It can be applied to accelerate several scientific computation applica-
762 tions, such as the DFT-based electronic structure calculations. To further improve the
763 numerical accuracy of the `PSelInv` method, especially for indefinite matrices, dynamic
764 pivoting strategies such as the Bunch-Kaufman procedure [Bunch and Kaufman 1977;
765 Grimes et al. 1994] for the factorization may be needed. Generalizing `PSelInv` to non-
766 symmetric matrices and combining it with other sparse direct solvers are other areas
767 in which we plan to work in the future.

768 ACKNOWLEDGMENTS

769 We would like to thank Xiaoye S. Li and François-Henry Rouet for helpful discussions.

770 REFERENCES

771 P. Amestoy, I. Duff, J.-Y. L'Excellent, and J. Koster. 2001. A fully asynchronous multifrontal solver using
772 distributed dynamic scheduling. *SIAM Journal on Matrix Analysis and Applications* 23, 15–41.

773 P. R. Amestoy, I. S. Duff, J.-Y. L'Excellent, Y. Robert, F.-H. Rouet, and B. Uçar. 2012b. On computing inverse
774 entries of a sparse matrix in an out-of-core environment. *SIAM Journal on Scientific Computing* 34,
775 A1975–A1999.

776 P. R. Amestoy, I. S Duff, J. Y. L'Excellent, and F. H. Rouet. 2012a. *Parallel Computation of Entries of* A^{-1}.
777 Technical Report. CERFACS, Toulouse, France.

778 C. Ashcraft and R. Grimes. 1989. The influence of relaxed supernode partitions on the multifrontal method.
779 *ACM Transactions on Mathematical Software* 15, 291–309.

780 C. Bekas, A. Curioni, and I. Fedulova. 2009. Low cost high performance uncertainty quantification. In
781 *Proceedings of the 2nd Workshop on High Performance Computational Finance*. 8.

782 C. Bekas, E. Kokiopoulou, and Y. Saad. 2007. An estimator for the diagonal of a matrix. *Applied Numerical*
783 *Mathematics* 57, 1214–1229.

784 L. S. Blackford. 1997. *ScaLAPACK User's Guide*. Vol. 4. SIAM.

785 J. R. Bunch and L. Kaufman. 1977. Some stable methods for calculating inertia and solving symmetric linear
786 systems. *Mathematics of Computation* 31, 137, 163–179.

787 Y. E. Campbell and T. A. Davis. 1995. *Computing the Sparse Inverse Subset: An Inverse Multifrontal Approach*.
788 Technical Report TR-95-021. University of Florida.

789 S. Cauley, V. Balakrishnan, G. Klimeck, and C.-K. Koh. 2012. A two-dimensional domain decomposition
790 technique for the simulation of quantum-scale devices. *Journal of Computational Physics* 231, 4, 1293–
791 1313.

792 C. Chevalier and F. Pellegrini. 2008. PT-scotch: A tool for efficient parallel graph ordering. *Parallel Computing*
793 34, 318–331.

794 T. A. Davis and Y. Hu. 2011. The University of Florida sparse matrix collection. *ACM Transactions on*
795 *Mathematical Software* 38, 1.

796 I. Duff, R. Grimes, and J. Lewis. 1992. *User's Guide for the Harwell-Boeing Sparse Matrix Collection*. Research
797 and Technology Division, Boeing Computer Services, Seattle, WA.

S. Eastwood and J. Wan. 2013. Finding off-diagonal entries of the inverse of a large symmetric sparse matrix. *Numerical Linear Algebra with Applications* 20, 1, 74–92. 798 799

A. Erisman and W. Tinney. 1975. On computing certain elements of the inverse of a sparse matrix. *Communications of the ACM* 18, 177. 800 801

G. H. Golub and C. F. Van Loan. 1996. *Matrix Computations* (3rd ed.). Johns Hopkins University Press, Baltimore, MD. 802 803

R. G. Grimes, J. G. Lewis, and H. D. Simon. 1994. A shifted block Lanczos algorithm for solving sparse symmetric generalized eigenproblems. *SIAM Journal on Matrix Analysis and Applications* 15, 1, 228–272. 804 805 806

U. Hetmaniuk, Y. Zhao, and M. P. Anantram. 2013. A nested dissection approach to modeling transport in nanodevices: Algorithms and applications. *International Journal for Numerical Methods in Engineering* 95, 7, 587–607. 807 808 809

P. Hohenberg and W. Kohn. 1964. Inhomogeneous electron gas. *Physical Review* 136, B864–B871. 810

M. Jacquelin, L. Lin, and C. Yang. 2014. *PSelInv*—A Distributed Memory Parallel Algorithm for Selected Inversion: The Symmetric Case. Technical Report, Lawrence Berkeley National Laboratory, Berkeley, CA. 811 812 813

G. Karypis and V. Kumar. 1998. A parallel algorithm for multilevel graph partitioning and sparse matrix ordering. *Journal of Parallel and Distributed Computing* 48, 71–85. 814 815

W. Kohn and L. Sham. 1965. Self-consistent equations including exchange and correlation effects. *Physical Review* 140, A1133–A1138. 816 817

G. Kotliar, S. Y. Savrasov, K. Haule, V. S. Oudovenko, O. Parcollet, and C. A. Marianetti. 2006. Electronic structure calculations with dynamical mean-field theory. *Review of Modern Physics* 78, 865–952. 818 819

A. Kuzmin, M. Luisier, and O. Schenk. 2013. Fast methods for computing selected elements of the Green's function in massively parallel nanoelectronic device simulations. In *Euro-Par 2013 Parallel Processing*. Lecture Notes in Computer Science, Vol. 8097. Springer, 533–544. 820 821 822

C. Lanczos. 1950. An iteration method for the solution of the eigenvalue problem of linear differential and integral operators. *Journal of Research of the National Bureau of Standards* 45, 255–282. 823 824

S. Li, S. Ahmed, G. Klimeck, and E. Darve. 2008. Computing entries of the inverse of a sparse matrix using the FIND algorithm. *Journal of Computational Physics* 227, 9408–9427. 825 826

Song Li and Eric Darve. 2012. Extension and optimization of the FIND algorithm: Computing Green's and less-than Green's functions. *Journal of Computational Physics* 231, 4, 1121–1139. 827 828

S. Li, W. Wu, and E. Darve. 2013. A fast algorithm for sparse matrix computations related to inversion. *Journal of Computational Physics* 242, 915–945. 829 830

X. S. Li and J. W. Demmel. 2003. SuperLU_DIST: A scalable distributed-memory sparse direct solver for unsymmetric linear systems. *ACM Transactions on Mathematical Software* 29, 110. 831 832

L. Lin, M. Chen, C. Yang, and L. He. 2013. Accelerating atomic orbital-based electronic structure calculation via pole expansion and selected inversion. *Journal of Physics: Condensed Matter* 25, 295501. 833 834

L. Lin, J. Lu, L. Ying, R. Car, and W. E. 2009b. Fast algorithm for extracting the diagonal of the inverse matrix with application to the electronic structure analysis of metallic systems. *Communications in Mathematical Sciences* 7, 755. 835 836 837

L. Lin, J. Lu, L. Ying, and E. Weinan. 2009a. Pole-based approximation of the Fermi-Dirac function. *Chinese Annals of Mathematics, Series B* 30, 729. 838 839

L. Lin, J. Lu, L. Ying, and E. Weinan. 2012. Adaptive local basis set for Kohn-Sham density functional theory in a discontinuous Galerkin framework I: Total energy calculation. *Journal of Computational Physics* 231, 2140–2154. 840 841 842

L. Lin, C. Yang, J. Lu, L. Ying, and E. Weinan. 2011a. A fast parallel algorithm for selected inversion of structured sparse matrices with application to 2D electronic structure calculations. *SIAM Journal on Scientific Computing* 33, 1329. 843 844 845

L. Lin, C. Yang, J. Meza, J. Lu, L. Ying, and E. Weinan. 2011b. SelInv—an algorithm for selected inversion of a sparse symmetric matrix. *ACM Transactions on Mathematical Software*, 40. 846 847

J. Liu. 1990. The role of elimination trees in sparse factorization. *SIAM Journal on Matrix Analysis and Applications* 11, 134. 848 849

D. E. Petersen, S. Li, K. Stokbro, H. H. B. Sørensen, P. C. Hansen, S. Skelboe, and E. Darve. 2009. A hybrid method for the parallel computation of Green's functions. *Journal of Computational Physics* 228, 5020–5039. 850 851 852

E. Rothberg and A. Gupta. 1994. An efficient block-oriented approach to parallel sparse Cholesky factorization. *SIAM Journal on Scientific Computing* 15, 1413–1439. 853 854

855 O. Schenk and K. Gartner. 2006. On fast factorization pivoting methods for symmetric indefinite systems.
856 *Electronic Transactions on Numerical Analysis* 23, 158–179.
857 R. B. Sidje and Y. Saad. 2011. Rational approximation to the Fermi-Dirac function with applications in
858 density functional theory. *Numerical Algorithms* 56, 455.
859 J. M. Soler, E. Artacho, J. D. Gale, A. García, J. Junquera, P. Ordejón, and D. Sánchez-Portal. 2002. The
860 SIESTA method for ab initio order-n materials simulation. *Journal of Physics: Condensed Matter* 14,
861 2745–2779.
862 K. Takahashi, J. Fagan, and M. Chin. 1973. Formation of a sparse bus impedance matrix and its application
863 to short circuit study. In *Proceedings of the 8th PICA Conference.*
864 J. M. Tang and Y. Saad. 2012. A probing method for computing the diagonal of a matrix inverse. *Numerical*
865 *Linear Algebra with Applications* 19, 485–501.
866 C. Vömel. 2010. ScaLAPACK's MRRR algorithm. *ACM Transactions on Mathematical Software* 37, 1.
867 Z. Xu and A. C. Maggs. 2013. Solving fluctuation-enhanced Poisson-Boltzmann equations. arXiv:1310.4682.

Received April 2014; revised May 2015; accepted May 2015

QUERIES

Q1: AU: Please provide full mailing and email addresses for all authors per ACM style.
Q2: AU: Throughout, please note that "LU" is sometimes italicized in text (same with "LDL"). Streamline style?
Q3: AU: The URL in footnot 1 redirects. Update?
Q4: AU: Please confirm position of closing parenthesis in the Output section of Algorithm 1.
Q5: AU: Add a comma before "gives," or delete comma after "lists"?
Q6: AU: Streamline font of terms such as "MUMPS"?